

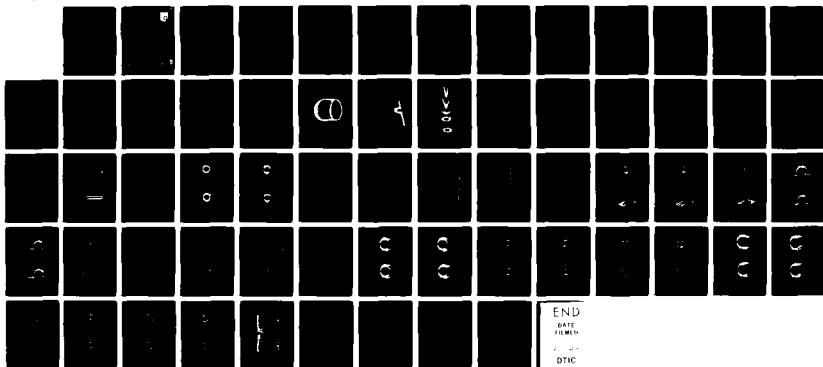
AD-A128 686

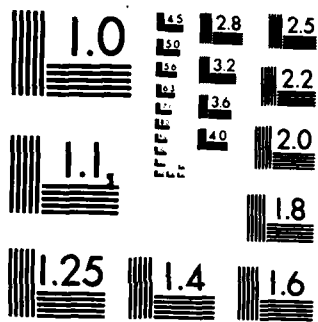
NUMERICAL SIMULATION OF FLOW AROUND A THREE-DIMENSIONAL
TURRET(U) DAYTON UNIV OH RESEARCH INST S C PUGHIT
NOV 82 UDR-TR-82-73 AFWAL-TR-82-3075 F33615-79-C-3030
F/G 12/1

1/1

UNCLASSIFIED

NL





MICROCOPY RESOLUTION TEST CHART
NATIONAL BUREAU OF STANDARDS-1963-A

2

AFWAL-TR-82-3075



AD A 128686

NUMERICAL SIMULATION OF FLOW AROUND A
THREE-DIMENSIONAL TURRET

S. C. PUROHIT
UNIVERSITY OF DAYTON RESEARCH INSTITUTE
300 COLLEGE PARK AVENUE
DAYTON, OHIO 45469

NOVEMBER 1982

FINAL REPORT FOR PERIOD MAY 1981 - APRIL 1982

APPROVED FOR PUBLIC RELEASE; DISTRIBUTION UNLIMITED.

DTIC FILE COPY

FLIGHT DYNAMICS LABORATORY
AIR FORCE WRIGHT AERONAUTICAL LABORATORIES
AIR FORCE SYSTEMS COMMAND
WRIGHT-PATTERSON AIR FORCE BASE, OHIO 45433

DTIC
ELECTE
MAY 31 1983
S E D

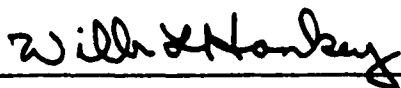
83 05 27 066

NOTICE

When Government drawings, specifications, or other data are used for any purpose other than in connection with a definitely related Government procurement operation, the United States Government thereby incurs no responsibility nor any obligation whatsoever; and the fact that the government may have formulated, furnished, or in any way supplied the said drawings, specifications, or other data, is not to be regarded by implication or otherwise as in any manner licensing the holder or any other person or corporation, or conveying any rights or permission to manufacture use, or sell any patented invention that may in any way be related thereto.

This report has been reviewed by the Office of Public Affairs (ASD/PA) and is releasable to the National Technical Information Service (NTIS). At NTIS, it will be available to the general public; including foreign nations.

This technical report has been reviewed and is approved for publication.



Project Engineer



LOWELL C. KEEL, Lt Col, USAF
Chief, Aerodynamics and Airframe Branch

FOR THE COMMANDER



JOHN R. CHEVALIER, Col, USAF
Chief, Aeromechanics Division

"If your address has changed, if you wish to be removed from our mailing list, or if the addressee is no longer employed by your organization please notify AFWAL/FIMM, W-PAFB, OH 45433 to help us maintain a current mailing list".

Copies of this report should not be returned unless return is required by security considerations, contractual obligations, or notice on a specific document.

Unclassified

SECURITY CLASSIFICATION OF THIS PAGE (When Data Entered)

REPORT DOCUMENTATION PAGE		READ INSTRUCTIONS BEFORE COMPLETING FORM
1. REPORT NUMBER AFWAL-TR-82-3075	2. GOVT ACCESSION NO. AD-A128686	3. RECIPIENT'S CATALOG NUMBER
4. TITLE (and Subtitle) NUMERICAL SIMULATION OF FLOW AROUND A THREE-DIMENSIONAL TURRET	5. TYPE OF REPORT & PERIOD COVERED Final, 18 May 1981 - 30 April 1982	
	6. PERFORMING ORG. REPORT NUMBER UDR-TR-82-73	
7. AUTHOR(s) S. C. Purohit	8. CONTRACT OR GRANT NUMBER(s) F33615-79-C-3030	
9. PERFORMING ORGANIZATION NAME AND ADDRESS University of Dayton Research Institute 300 College Park Avenue Dayton, Ohio 45469	10. PROGRAM ELEMENT, PROJECT, TASK AREA & WORK UNIT NUMBERS PE/JON: 61102F/ 2307N603	
11. CONTROLLING OFFICE NAME AND ADDRESS Flight Dynamics Laboratory (AFWAL/FIMM) AF Wright Aeronautical Laboratories (AFSC) Wright-Patterson AFB, Ohio 45433	12. REPORT DATE November 1982	
	13. NUMBER OF PAGES 53	
14. MONITORING AGENCY NAME & ADDRESS (if different from Controlling Office)	15. SECURITY CLASS. (of this report) Unclassified	
	15a. DECLASSIFICATION/DOWNGRADING SCHEDULE	
16. DISTRIBUTION STATEMENT (of this Report) Approved for public release; distribution unlimited.		
17. DISTRIBUTION STATEMENT (of the abstract entered in Block 20, if different from Report)		
18. SUPPLEMENTARY NOTES		
19. KEY WORDS (Continue on reverse side if necessary and identify by block number) Flow field structure over a turret; unsteady three-dimensional numerical Navier-Stokes solutions; turbulent flow; separation flow; wake dynamics; RMS values		
20. ABSTRACT (Continue on reverse side if necessary and identify by block number) The compressible Navier-Stokes equations in mass averaged vari- ables are numerically solved for flow around a surface mounted turret. The three-dimensional unsteady separated flow is investigated with emphasis on the near wake region. The compu- tation is performed on the CRAY-1 computer using MacCormack's explicit finite difference scheme. For the free stream Mach number 0.55 and Reynolds number $10.3 \times 10^5/m$, the time dependent $1,000,000/m$		

Unclassified

SECURITY CLASSIFICATION OF THIS PAGE(When Data Entered)

20. calculation is carried out for 55,800 grid points in the computational domain to achieve steady state periodic solution. The entire flow field around the turret is analyzed and the comparison with available experimental data is reported.

Unclassified

SECURITY CLASSIFICATION OF THIS PAGE(When Data Entered)

ACKNOWLEDGEMENT

The author acknowledges the support provided by Lt. Col. John J. Russell and Capt. Richard K. deJonckheere of the Air Force Weapons Laboratory at Kirtland Air Force Base for the use of the CRAY-1 computer. The author is also indebt to Dr. W. L. Hankey, Jr. and Dr. J. S. Shang for their stimulating and useful discussion.

The one-year stay with the University of Dayton Research Institute, under the Visiting Scientist Program, was made meaningful and productive through the timely advises and continued help from Mr. Dale H. Whitford and Dr. James N. Scott. Their support is duly acknowledged with appreciation.

This work was performed during the author's study leave from the Aeronautics Group, Vikram Sarabhai Space Centre, Indian Space Research Organisation, Trivandrum, India. The encouragement to conduct research by The Government of India is gratefully acknowledged.

Accession For	
NTIS GRA&I	<input checked="" type="checkbox"/>
DTIC TAB	<input type="checkbox"/>
Unannounced	<input type="checkbox"/>
Justification	
By _____	
Distribution/	
Availability Codes	
Dist	Avail and/or Special
A	



TABLE OF CONTENTS

<u>SECTION</u>		<u>PAGE</u>
1	INTRODUCTION	1
2	ANALYSIS	3
	Eddy Viscosity Model	12
3	NUMERICAL PROCEDURE	14
4	RESULTS AND DISCUSSIONS	16
5	CONCLUSIONS	51
	REFERENCES	52

LIST OF ILLUSTRATIONS

<u>FIGURE</u>		<u>PAGE</u>
1	The Turret	6
2	Mesh Point Distribution on the Turret	8
3	Mesh Points in the Plane 0° - 180°	9
4	Mesh Distribution at Selected Stations	10
5	Boundary Conditions	11
6	Comparison of Pressure Distribution (a) At the turret shoulder (b) On the hemispherical surface, 45° MPA	17
7	Instantaneous Pressure Distribution Contours Around the Turret	18
8	Instantaneous Limiting Streamline Pattern on the Flat Surface at Different Times (a) $T/T_{CH} = 5.1488$ (b) $T/T_{CH} = 9.1799$ (c) $T/T_{CH} = 13.0183$ (d) $T/T_{CH} = 17.7505$	20 20 21 21
9	Mach Number Distribution (a) Close to the flat surface (b) At the turret shoulder	23
10	RMS Density Fluctuations for the 90° Azimuth Angle	24
11	Peak RMS Density Fluctuation at Various Turret Window Heights	25
12	RMS Density Fluctuation Contours and Planar Plots (a) Contours of the RMS density fluctuations for $Y/R = 0.4479$ (aa) Planar plot of the RMS density fluctuations for $Y/R = 0.4479$ (b) Contours of the RMS density fluctuations for $Y/R = 1.0786$ (bb) Planar plot of the RMS density fluctuations for $Y/R = 1.0786$ (c) Contours of the RMS density fluctuations for $Y/R = 1.6490$ (cc) Planar plot of the RMS density fluctuations for $Y/R = 1.6490$	27 27 28 28 29 29

LIST OF ILLUSTRATIONS (Continued)

<u>FIGURE</u>		<u>PAGE</u>
13	Velocity Field in the Cross-sectional Plane at Different Times	
	(a) $T/T_{CH} = 5.1488$	30
	(b) $T/T_{CH} = 9.1799$	30
	(c) $T/T_{CH} = 13.0183$	31
	(d) $T/T_{CH} = 17.7505$	31
14	Mach Number Contours in the Cross-sectional Plane at Different Times	
	(a) $T/T_{CH} = 5.1488$	32
	(b) $T/T_{CH} = 9.1799$	32
	(c) $T/T_{CH} = 13.0183$	33
	(d) $T/T_{CH} = 17.7505$	33
15	Density Contours in the Cross-sectional Plane at Different Times	
	(a) $T/T_{CH} = 5.1488$	34
	(b) $T/T_{CH} = 9.1799$	34
	(c) $T/T_{CH} = 13.0183$	35
	(d) $T/T_{CH} = 17.7505$	35
16	Velocity Field Around the Turret at $\frac{Y}{R} = 0.3543$ at Different Times	
	(a) $T/T_{CH} = 5.1488$	37
	(b) $T/T_{CH} = 9.1799$	37
	(c) $T/T_{CH} = 13.0183$	38
	(d) $T/T_{CH} = 17.7505$	38
17	Mach Number Contours Around the Turret at $\frac{Y}{R} =$ 0.3543 at Different Times	
	(a) $T/T_{CH} = 5.1488$	39
	(b) $T/T_{CH} = 9.1799$	39
	(c) $T/T_{CH} = 13.0183$	40
	(d) $T/T_{CH} = 17.7505$	40
18	Density Contours Around the Turret at $\frac{Y}{R} =$ 0.3543	
	(a) $T/T_{CH} = 5.1488$	41
	(b) $T/T_{CH} = 9.1799$	41
	(c) $T/T_{CH} = 13.0183$	42
	(d) $T/T_{CH} = 17.7505$	42

LIST OF ILLUSTRATIONS (Concluded)

<u>FIGURE</u>		<u>PAGE</u>
19	Velocity Field Around the Turret Shoulder at Different Times	
	(a) $T/T_{CH} = 5.1488$	43
	(b) $T/T_{CH} = 9.1799$	43
	(c) $T/T_{CH} = 13.0183$	44
	(d) $T/T_{CH} = 17.7505$	44
20	Mach Number Contours Around the Turret Shoulder at Different Times	
	(a) $T/T_{CH} = 5.1488$	45
	(b) $T/T_{CH} = 9.1799$	45
	(c) $T/T_{CH} = 13.0183$	46
	(d) $T/T_{CH} = 17.7505$	46
21	Density Contours Around the Turret Shoulder at Different Times	
	(a) $T/T_{CH} = 5.1488$	47
	(b) $T/T_{CH} = 9.1799$	47
	(c) $T/T_{CH} = 13.0183$	48
	(d) $T/T_{CH} = 17.7505$	48
22	Instantaneous Limiting Streamline Pattern on the Turret Surface	49

NOMENCLATURE

AZA	Azimuth angle around turret
CP	Pressure coefficient
D	Turret diameter
e	Specific energy
e_i	Specific internal energy, $C_v \cdot T$
F, G, H	Vector fluxes in mean flow equations
J	Jacobian of coordinate transformation
ΔL	Arc length
N	Singular point, node
P	Pressure
P_r	Molecular Prandtl number, 0.72
P_{rt}	Turbulent Prandtl number, 0.90
R	Turret radius
S	Singular point, saddle point
t	Time
T_{CH}	Characteristics time, D/U_∞
u, v, w	Velocity components in cartesian coordinates
U	Mass averaged dependent variable
U_{max}	Maximum velocity in near wake
x, y, z	Cartesian coordinates
ρ	Density
ξ, η, ζ	Transformed coordinates
ϵ	Eddy viscosity
γ	Ratio of specific heats
μ	Molecular viscosity coefficient
δ_i^*	Kinematic displacement thickness
ω	Vorticity

Subscripts

∞	Free stream condition
w	Surface condition

SECTION 1
INTRODUCTION

The understanding and analysis of three-dimensional fluid behavior around a surface mounted blunt obstacle (turret) is of considerable importance for flight applications. The prime motivation to solve such problems has been to investigate the basic phenomenon of separated flow and to determine the associated forces on the object. In addition, the dynamic features of the unsteady flow field around the obstacle are of interest to the designer.

The time variation of the separation line due to the shedding of vortices for the flow past a turret produces a complex and intriguing flow structure. Also the appropriate turbulence model, ranges of Mach number and Reynolds number, and protuberance height are some of the elements in parametric space which restrict the unified approach and generality of the solution. The experimental and computational approaches are the common aerodynamics tools to investigate complex problems. However, during recent years, the computational approach has been preferred because of its lower cost, availability of faster computers, and detailed description of the fluid physics. In this frame of reference, the present work addresses the "computational flow visualization" of the three-dimensional separated flow. The primary objective is to provide an efficient numerical procedure for the solution of the governing equations and to compare the computed results with the previously obtained experimental data.

A survey of the literature reveals a substantial but not an exhaustive effort in this area. The experimental results^[1-5] obtained primarily by conventional flow visualization techniques and the data correlated indicate some important facts about the primary separation features for flow past small protuberances. For different protuberance heights, the available flow field data is so sparse that its interpretation leading to a general conclusion

is not obvious. To acquire the finer details, it is felt that the three-dimensional separated flow past a turret requires numerical analysis.

Influenced by the results of experimental studies and a search for proper criterion for three-dimensional flow separation led to a simple convincing topological approach^[6-9]. This approach is based on the hypothesis that vector fields of the skin friction lines and external streamlines remain continuous. Taking bodies of revolution at various angles of incidence, for example, it was possible to synthesize the flow mechanism in a rational manner. We will be using some of these topological ideas to explain the fluid behavior around the turret.

Turning to our present effort, for subsonic high Reynolds number flow, past a hemispherically capped cylindrical obstacle (the turret), the horseshoe vortex, turbulent boundary layer characteristics and near wake structure, need careful attention, particularly from a numerical simulation point of view. A subset of this immense problem, unsteady flow oscillations past a circular cylinder, was recently studied by Shang^[10]. For this numerical experiment, the mesh point distribution and appropriate boundary conditions were optimized to yield the time mean and fluctuating properties of the fluid. This two-dimensional computation provided encouragement to continue further and to analyze the large-scale organized fluid motion around a three-dimensional turret at a Mach number of 0.55 and a Reynolds number of $10.3 \times 10^6/m$. At these conditions the turret height is much larger than that of the turbulent boundary layer on the surface. The aim is to evaluate the density data field and its fluctuations around the turret and compare the results with the experimental data of deJonckheere, et al.^[11]

SECTION 2
ANALYSIS

For the problem under consideration, the solution of unsteady compressible Navier-Stokes equations becomes necessary. These equations offer, on a fine scale, a good insight into the viscous-inviscid interaction and the separated flow structure. For the present Reynolds number range, the flow along the flat plate as well as around the turret will be turbulent, and, thus, adequate inclusion of turbulence terms is needed. In the absence of body forces and electromagnetic effects, the governing equations can be written as

$$\frac{\partial \rho}{\partial t} + \nabla \cdot (\rho \bar{u}) = 0$$

$$\frac{\partial (\rho \bar{u})}{\partial t} + \nabla \cdot (\rho \bar{u} \bar{u} - \bar{\tau}) = 0$$

$$\frac{\partial (\rho e)}{\partial t} + \nabla \cdot (\bar{q} - \bar{u} \cdot \bar{\tau}) = 0$$

where the heat flux \bar{q} is given by the Fourier's law

$$\bar{q} = -K \nabla T$$

and the shear stress tensor $\bar{\tau}$ is defined as

$$\bar{\tau}_{ij} = -(u+\epsilon) (\text{Def } \bar{u})_{ij} + \left(\frac{2}{3} (u+\epsilon) \nabla \cdot \bar{u} + p \right) \cdot \delta_{ij} \quad .$$

In order to optimize the numerical resolution, using body oriented coordinate transformation, these equations, in mass averaged variables, can be written in the following convenient form:

$$\begin{aligned} \frac{\partial \bar{U}}{\partial t} + \begin{bmatrix} \xi_x \\ \xi_y \\ \xi_z \end{bmatrix} \left(\frac{\partial \bar{F}}{\partial \xi}, \frac{\partial \bar{G}}{\partial \xi}, \frac{\partial \bar{H}}{\partial \xi} \right) + \begin{bmatrix} \eta_x \\ \eta_y \\ \eta_z \end{bmatrix} \left(\frac{\partial \bar{F}}{\partial \eta}, \frac{\partial \bar{G}}{\partial \eta}, \frac{\partial \bar{H}}{\partial \eta} \right) + \\ + \begin{bmatrix} \zeta_x \\ \zeta_y \\ \zeta_z \end{bmatrix} \left(\frac{\partial \bar{F}}{\partial \zeta}, \frac{\partial \bar{G}}{\partial \zeta}, \frac{\partial \bar{H}}{\partial \zeta} \right) = 0 \end{aligned} \quad (1)$$

where

$$\vec{U} = \begin{bmatrix} \rho \\ \rho u \\ \rho v \\ \rho w \\ \rho e \end{bmatrix} \quad (2)$$

$$\vec{F} = \begin{bmatrix} \rho u \\ \rho u^2 + \sigma_x \\ \rho uv + \tau_{xy} \\ \rho uw + \tau_{xz} \\ (\rho e + \sigma_x)u + \tau_{xy} \cdot v + \tau_{xz} \cdot w - \dot{q}_x \end{bmatrix} \quad (3)$$

$$\vec{G} = \begin{bmatrix} \rho v \\ \rho vu + \tau_{yx} \\ \rho v^2 + \sigma_y \\ \rho vw + \tau_{yz} \\ (\rho e + \sigma_y)v + \tau_{yx} \cdot u + \tau_{yz} \cdot w - \dot{q}_y \end{bmatrix} \quad (4)$$

$$\vec{H} = \begin{bmatrix} \rho w \\ \rho wu + \tau_{zx} \\ \rho wv + \tau_{zy} \\ \rho w^2 + \sigma_z \\ (\rho e + \sigma_z)w + \tau_{zx} \cdot u + \tau_{zy} \cdot v - \dot{q}_z \end{bmatrix} \quad (5)$$

$$\sigma_x = p + 2/3(\mu + \epsilon) \left(\frac{\partial u}{\partial x} + \frac{\partial v}{\partial y} + \frac{\partial w}{\partial z} \right) - 2(\mu + \epsilon) \cdot \frac{\partial u}{\partial x} \quad (6-1)$$

$$\tau_{xy} = \tau_{yx} = -(\mu + \epsilon) \left(\frac{\partial u}{\partial y} + \frac{\partial v}{\partial x} \right) \quad (6-2)$$

$$\tau_{xz} = \tau_{zx} = -(\mu + \epsilon) \left(\frac{\partial u}{\partial z} + \frac{\partial w}{\partial x} \right) \quad (6-3)$$

$$\sigma_y = p + 2/3(\mu + \epsilon) \left(\frac{\partial u}{\partial x} + \frac{\partial v}{\partial y} + \frac{\partial w}{\partial z} \right) - 2(\mu + \epsilon) \cdot \frac{\partial v}{\partial y} \quad (6-4)$$

$$\tau_{yz} = \tau_{zy} = -(\mu + \epsilon) \left(\frac{\partial v}{\partial z} + \frac{\partial w}{\partial y} \right) \quad (6-5)$$

$$\sigma_z = p + 2/3(\mu + \epsilon) \left(\frac{\partial u}{\partial x} + \frac{\partial v}{\partial y} + \frac{\partial w}{\partial z} \right) - 2(\mu + \epsilon) \cdot \frac{\partial w}{\partial z} \quad (6-6)$$

$$\dot{q}_x = \gamma \left(\frac{\mu}{P_r} + \frac{\epsilon}{P_{r_t}} \right) \cdot \frac{\partial e_i}{\partial x} \quad (7-1)$$

$$\dot{q}_y = \gamma \left(\frac{\mu}{P_r} + \frac{\epsilon}{P_{r_t}} \right) \cdot \frac{\partial e_i}{\partial y} \quad (7-2)$$

$$\dot{q}_z = \gamma \left(\frac{\mu}{P_r} + \frac{\epsilon}{P_{r_t}} \right) \cdot \frac{\partial e_i}{\partial z} \quad (7-3)$$

$$e = e_i + (u^2 + v^2 + w^2)/2.0 \quad (8)$$

This system of equations is closed by a perfect gas law, Sutherland's viscosity formula, and appropriate eddy viscosity model as a supplementary relation.

The fluid motion defined by the aforementioned set of equations is to be analyzed around a turret (Figure 1) mounted on a flat surface. Its base is a circular cylinder with diameter 0.44 meter and the height to diameter ratio 1.071. One of the sides has a cut-out (window) of area 0.249 meter \times 0.201 meter at a normal distance 0.194 meter from the turret axis. The top of the turret is a hemispherical dome of radius 0.223 meter whose center is on the axis. The ξ , η , ζ correspond to normal, axial, and tangential transformed coordinates of the turret, respectively, with its origin at the turret base. For this configuration, the experimental results^[11] were available for various locations of the turret window (look angle). In order to demonstrate, a typical flow field for a 90 degree look angle was simulated.

One of the major tasks in numerical simulation is the proper selection of mesh system in the computational domain. A judicious choice of grid points helps capture the important flow field characteristics as well as reducing the data processing time. After much study the following choice was made. The turret surface is defined by 62 \times 30 points. On the cylindrical portion, 15 points were used in the axial direction stretched exponentially from the base and 15 points were uniformly placed on the hemispherical dome. In the tangential direction, 62 equidistant

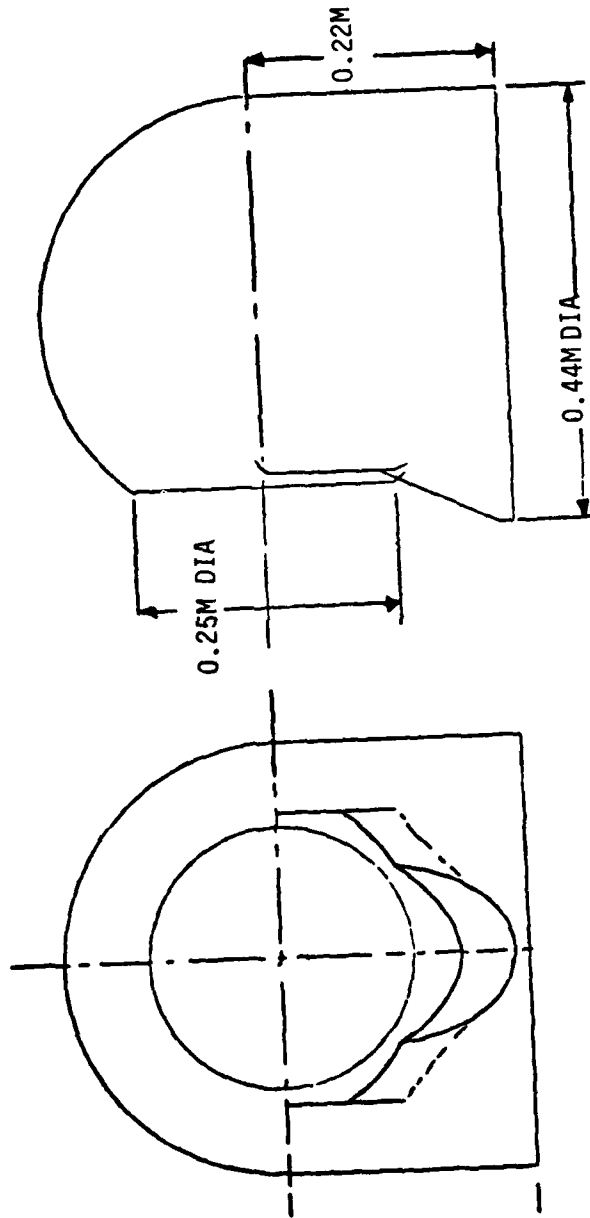


Figure 1. The Turret.

points were used with the first two points overlapping to permit the use of fourth order pressure damping (Figure 2). Using these surface nodes as the reference points, the normal coordinates are then described by 30 exponentially stretched points from the turret surface extending outward to ten times the turret radius (Figures 3 and 4). The finer mesh near the turret and flat plate will help resolve the viscous effects while the coarser mesh helps reduce the computational time. Care has been taken that no mesh point lies on the turret axis; however, a sufficient number of mesh points is provided to resolve the flow field. For this mesh arrangement, the derivatives of coordinate transformation can be evaluated through the Jacobian, J.

$$J = \begin{vmatrix} x_{\xi} & y_{\xi} & z_{\xi} \\ x_{\eta} & y_{\eta} & z_{\eta} \\ x_{\zeta} & y_{\zeta} & z_{\zeta} \end{vmatrix} .$$

This Jacobian of the coordinate transformation is a non-singular determinant and allows a one-to-one correspondence from the physical to the transformed space.

In any numerical algorithm, the boundary conditions play a crucial role in both the accuracy and stability of the numerical scheme. The initial and boundary conditions associated with this system of equations are straightforward and simple. Initially, the turret is assumed to be immersed completely in a uniform stream. The upstream boundary conditions are merely the free stream value, whereas at the downstream side, the gradient of properties is assumed to vanish. At the solid contours, the no slip conditions for velocity, ortho-isobaric condition for density and isothermal conditions are imposed; while near the turret axis, an interpolation is adopted to eliminate calculation on this singularity (Figure 5). Thus, for the independent variables, $0 \leq \xi, \eta, \zeta \leq 1$, in the computational domain, the conditions are set in the following forms.

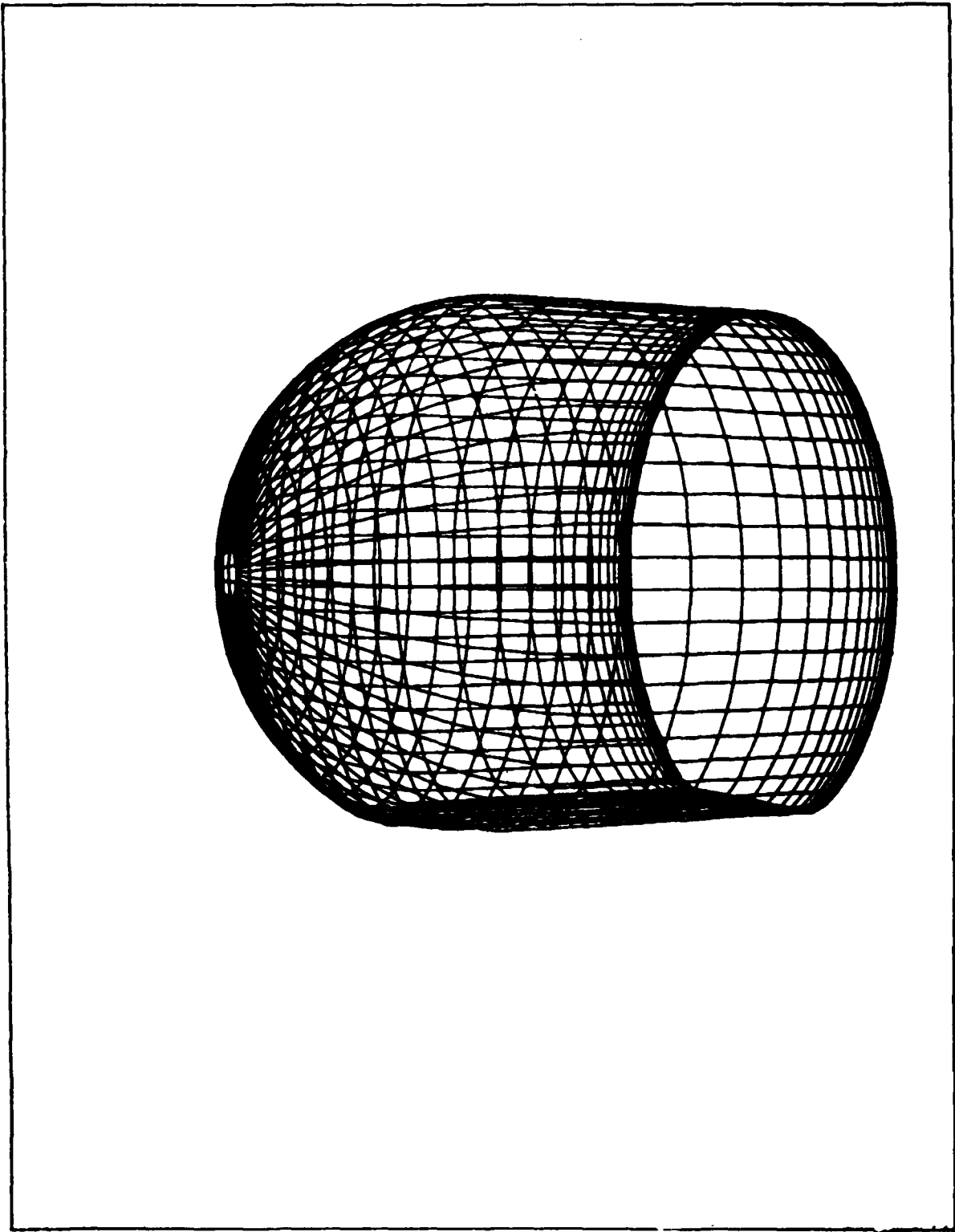


Figure 2. Mesh Point Distribution on the Turret.

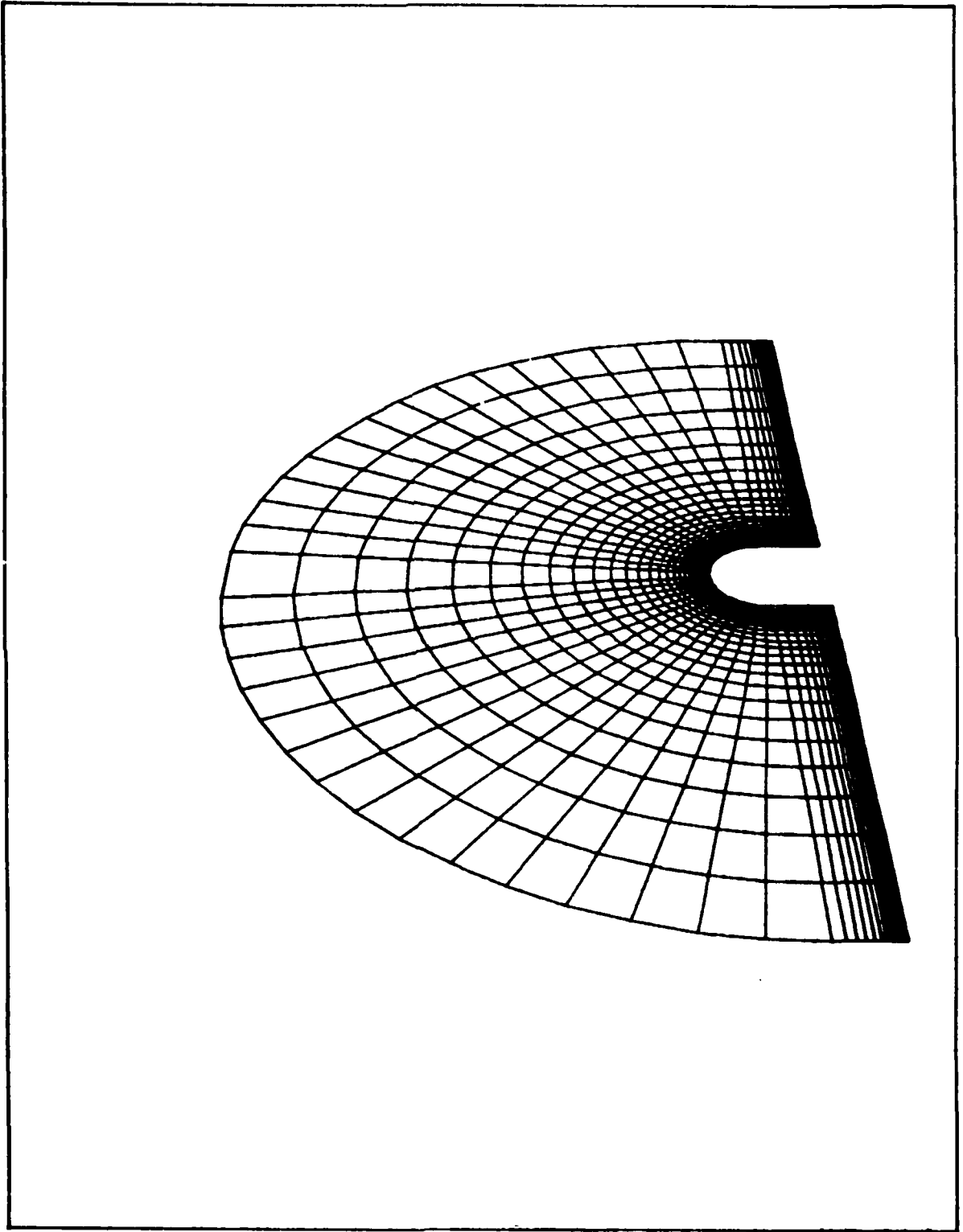


Figure 3. Mesh Points in the Plane $0^\circ - 180^\circ$.

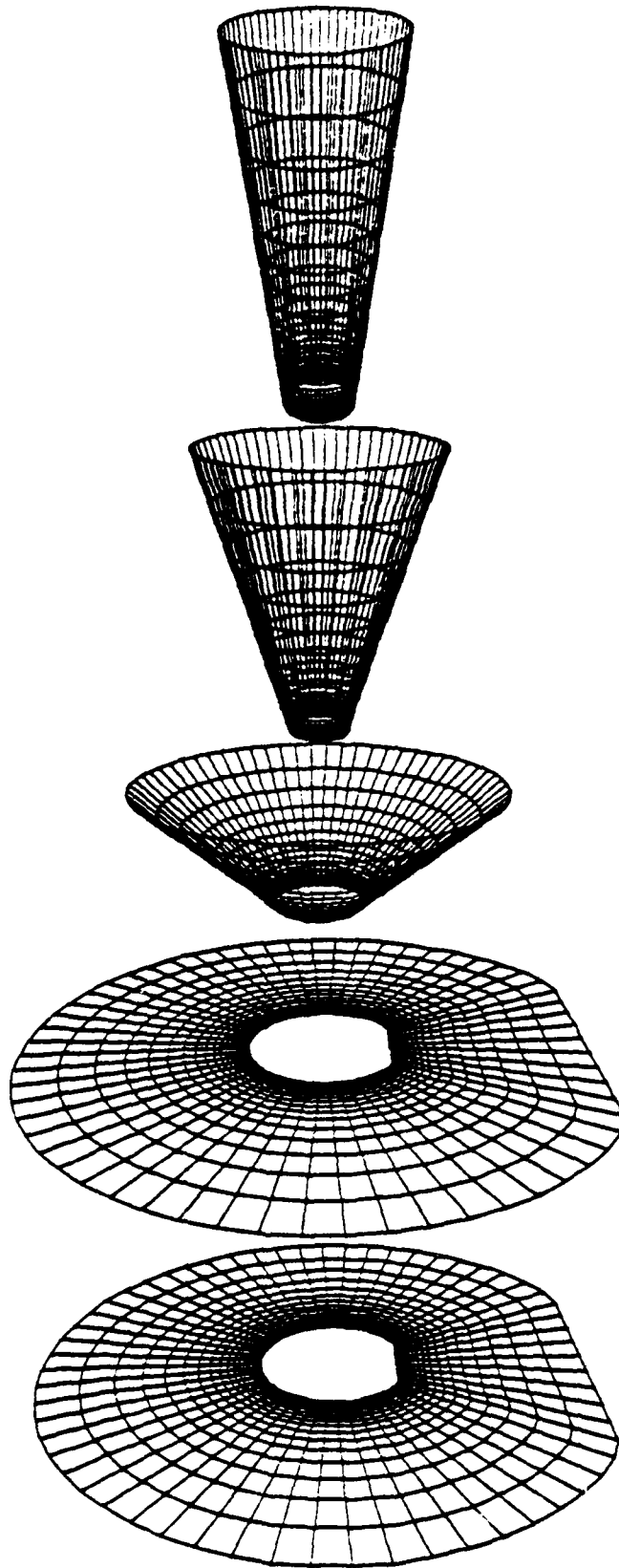


Figure 4. Mesh Distribution at Selected Stations.

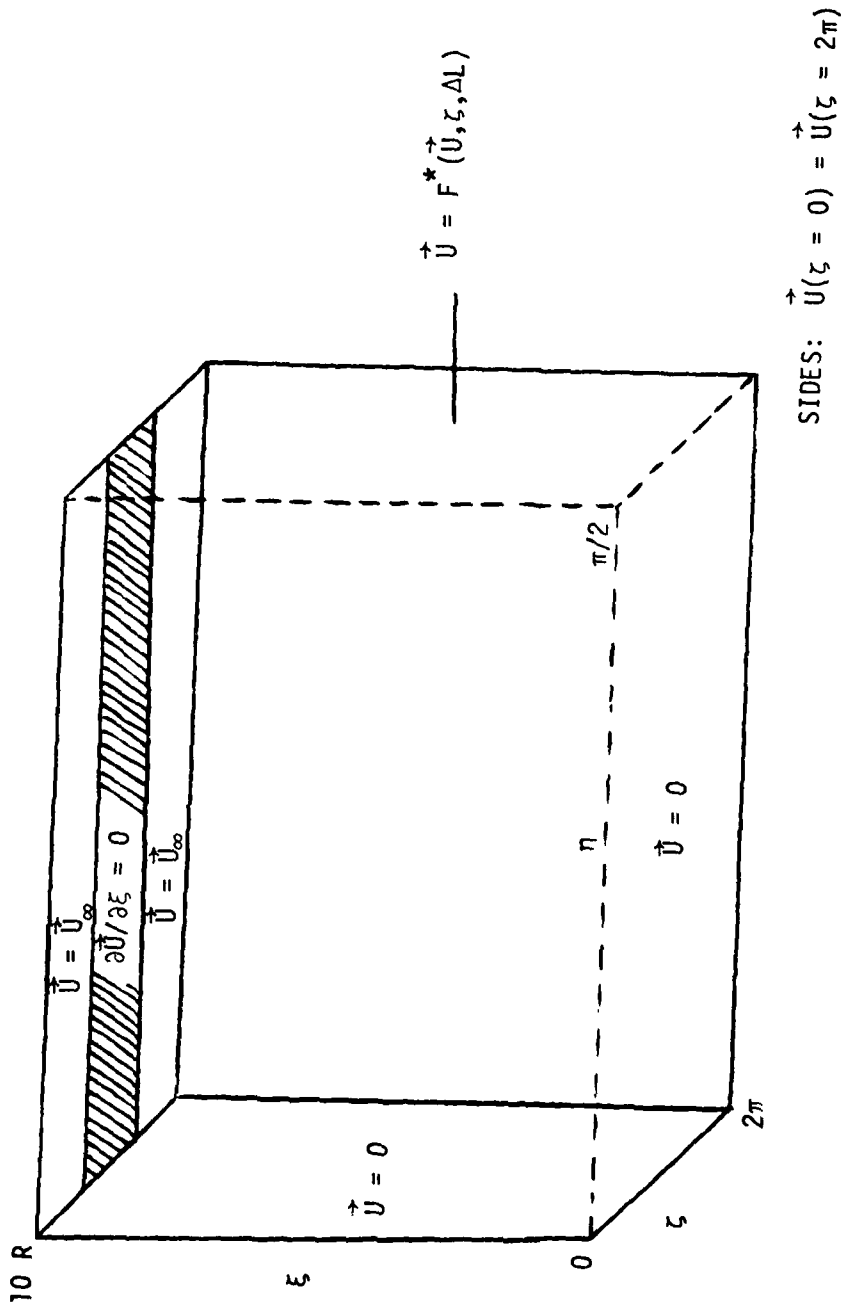


Figure 5. Boundary Conditions.

Initial Conditions

$$\vec{U}(0, \xi, \eta, \zeta) = \vec{U}_\infty(\xi, \eta, \zeta), \quad (9)$$

Boundary Conditions

$$\text{Upstream: } \vec{U}(t, \xi, 1, \zeta) = \vec{U}(t, \xi, 1, \zeta_0), \quad (10)$$

$$\zeta_1 < \zeta_0 < \zeta_2$$

$$\text{Downstream: } \frac{\partial}{\partial \xi} \vec{U}(t, \xi, \eta, \zeta_0) = 0 \quad (11)$$

$$\zeta_1 \geq \zeta_0 \geq \zeta_2$$

$$\text{At the Solid Contours, } \eta=0 \quad u = v = w = 0 \quad (12-1)$$

$$T = T_w = 1.0584T_\infty \quad (12-2)$$

$$\rho_w = \rho_\infty \cdot \frac{T_\infty}{T_w} \quad (12-3)$$

$$\text{At the Axis } \vec{U}(t, \xi, 1, \zeta) = F(\vec{U}(t, \xi, 1, \zeta_0), \zeta_1, \zeta_2, \Delta L) \quad (13)$$

where ζ_1 and ζ_2 are the extremum of the left half of the computational domain exposed to the free stream and ΔL is the arc length subtended by two consecutive points along the turret axis to the center of the hemisphere. The significant variation in the turret surface curvature and strong vortical interactions^[12] require careful selection of the turbulence model. Once the turbulence model is identified, the system of equations is closed and the computation can be initiated.

Eddy Viscosity Model

The closure of the system of equations is achieved by using a Cebeci-Smith type eddy viscosity model and by assigning a turbulent Prandtl number of 0.90. The specific turbulence model used is a simplified version due to Baldwin and Lomax^[13].

In the inner region:

$$\epsilon_i = \rho \cdot (K_1 \cdot L \cdot D_1)^2 \cdot |\omega| \quad (14)$$

where ω is the vorticity of the flow field. In the present formulation, the Van Driest's damping factor is given as

$$D_1 = 1 - \exp\left(-\sqrt{\frac{\rho_w \cdot |\omega_w|}{\mu_w}} \cdot L/26\right) \quad (15)$$

and the scaling length L is the distance measured along the outward normal from the surface.

In the wake region, we use the modified Clauser's law,

$$\epsilon_o = 0.00168 \cdot \rho_\infty \cdot U_{\max} \cdot \delta_i^* \quad (16)$$

where δ_i^* is the kinematic displacement thickness of the wake in the plane of the turret shoulder. This thickness is evaluated at a downstream distance about six times the turret radius.

$$\delta_i^* = \int_{\zeta_1}^{\zeta_2} \left(1 - \frac{u^2 + v^2 + w^2}{U_{\max}^2}\right) \cdot d\zeta \quad .$$

The effective eddy viscosity is, thus, taken to be

$$\epsilon = \min(\epsilon_o, \epsilon_i). \quad (17)$$

SECTION 3 NUMERICAL PROCEDURE

The present investigation utilizes the well established vector solver^[14, 15] which adopts, basically, the MacCormack's explicit finite difference scheme^[16]. Owing to the large memory availability and high data processing rate (the CPU time per grid point per time iteration), the CRAY-1 computer was chosen for our computation. The intricate interplay between its capacity and numerical scheme provided an efficient and powerful tool to analyze this three-dimensional problem with acceptable engineering accuracy.

We used the solver to initialize the planes or "pages" in the (η - ζ) plane and to sweep, for each time step, in the ξ -direction, thus minimizing the data flow from and to the disk or mass storage devices. The vector length for this case was 62, which is also the longest index array of the three-dimensional mesh system. The computational facilities were utilized with remote access via long distance dial-up and the SAMNET network link. The data processing rate of 6.8×10^{-5} seconds was achieved for the present analysis. Most of the available memory was required to perform the time dependent calculations.

The finer mesh sizes in the normal direction of the turret and flat surface were 0.357×10^{-2} meter and 0.345×10^{-2} meter, respectively, and the angular displacement between nodes was six degrees (6°). These mesh sizes seem to provide satisfactory time step increments during the computation. Further refinement could result in the stiffened behavior of the transformation metric element near the dome and/or much smaller time step. A conservative choice of the Courant-Fredrich-Lewy (CFL) condition was implemented to have optimum time step with stable numerical evolution.

Once the initial phase of computation was completed and some anticipated periodicity in the flow characteristics was observed, the evaluation of the root mean square (RMS) density fluctuation was attempted. For turbulent compressible flow, separating the

time mean and fluctuations of density, the squared density fluctuation over a characteristic time period was calculated as

$$\langle \rho'^2 \rangle = \frac{1}{T_p} \int_t^{t+T_p} \rho^2 \cdot dt - \left[\frac{1}{T_p} \int_t^{t+T_p} \rho \cdot dt \right]^2 \quad (18)$$

where T_p is the principal time period, equal to 0.0114 seconds and is a function of Strouhal number, turret diameter and free stream velocity. The computation of RMS density for all grid points demanded three times the additional available computer memory which was not feasible at this stage. Therefore, this particular analysis was confined to a part of the computational domain from a turret height $\frac{Y}{R} = 0.4$ to $\frac{Y}{R} = 1.7$. A total of 9880.0 seconds CPU time of CRAY-1 computer were required (using a CRAY FORTRAN compiler (CFT) version 1.09) to calculate the entire flow and the RMS density fluctuations over one principal period. Almost "all" the memory resources of the computer were required to process the three-dimensional separated flow.

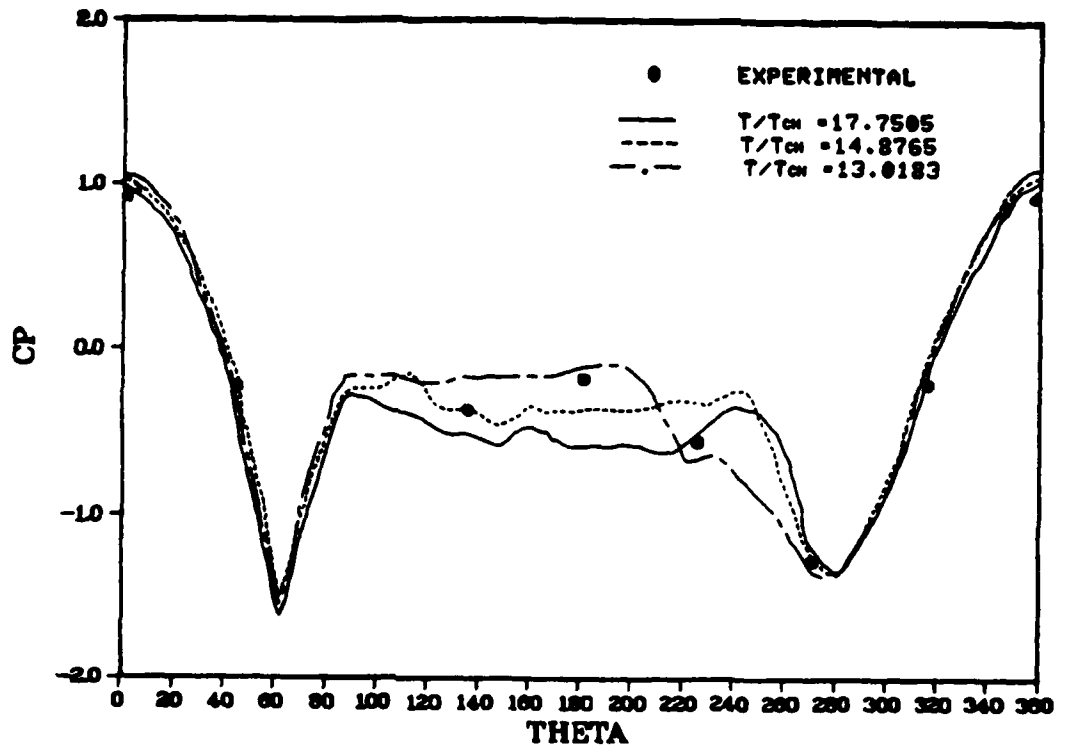
SECTION 4

RESULTS AND DISCUSSIONS

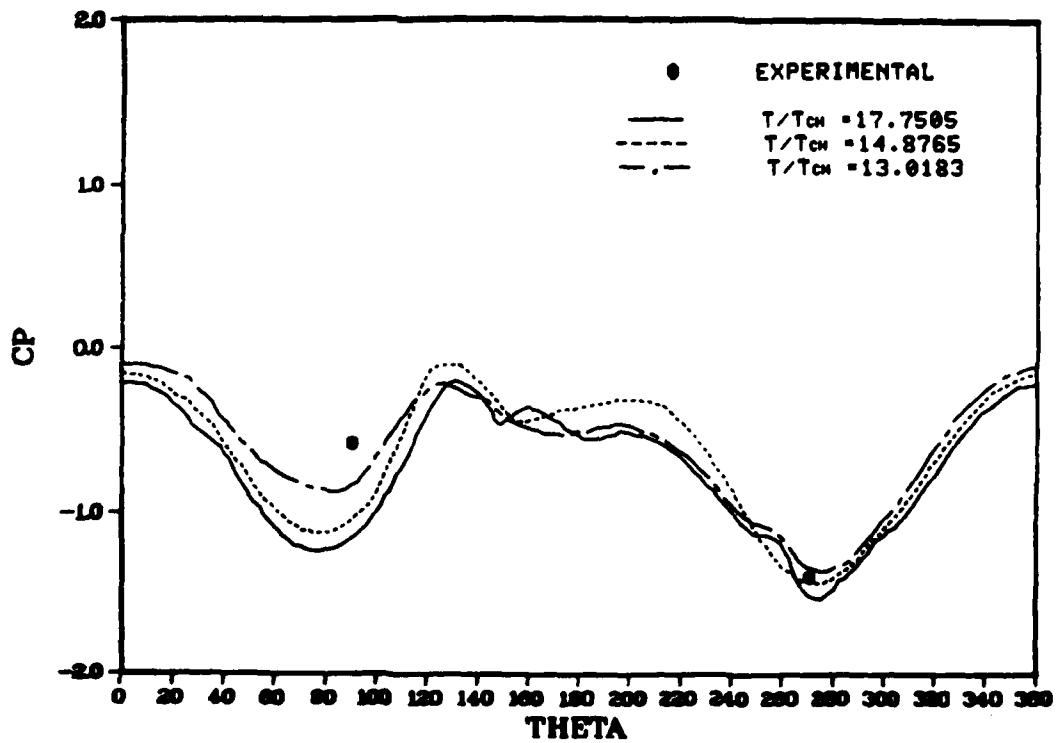
This section contains two main areas of discussion. The first of these will deal with the comparison of the computed and experimental results^[11]. This permits the validation of our computational procedure as well as providing guidelines for the subsequent analysis. The rest of the discussion is concentrated on probing into the different aspects of three-dimensional separated flow structure.

The pressure coefficient distribution at the turret shoulder and 45° meridian plane angle (MPA) are presented in Figure 6. The variable THETA is the azimuth angle measured clockwise from the oncoming free stream direction. Thus, the cavity side of the turret is located in the range 0° to 180° and the smooth side is between 180° and 360° . We will adhere to the same definition throughout our discussion. The comparison shows good agreement with the experimental results. The different curves represent the variation in pressure coefficient during one principal time period. At the turret shoulder, where the cylindrical and hemispherical surfaces meet, the computed mean CP (Figure 6a) is 0.9918 for the forward stagnation point (AZA = 0°), whereas the measured value is 0.91. The front edge of the turret window experiences a sudden expansion of the flow and a small separation zone resulting in a steep drop in pressure (AZA = 63°) and a rapid pressure recovery within 20° in the downstream direction. The smooth side does not witness such abrupt changes and gives way to minimum pressure value at AZA = 279° . For the 45° MPA, on the hemispherical surface (Figure 6b), the CP distribution exhibits relatively smooth variation. It also hints that the presence of the turret window has very small effects for this meridian plane.

This argument is further confirmed by Figure 7, which shows the instantaneous pressure distribution contours of different levels around the turret surface. A zone of very low pressure can



(a) At the turret shoulder.



(b) On the hemispherical surface, 45° MPA.
Figure 6. Comparison of Pressure Distribution.

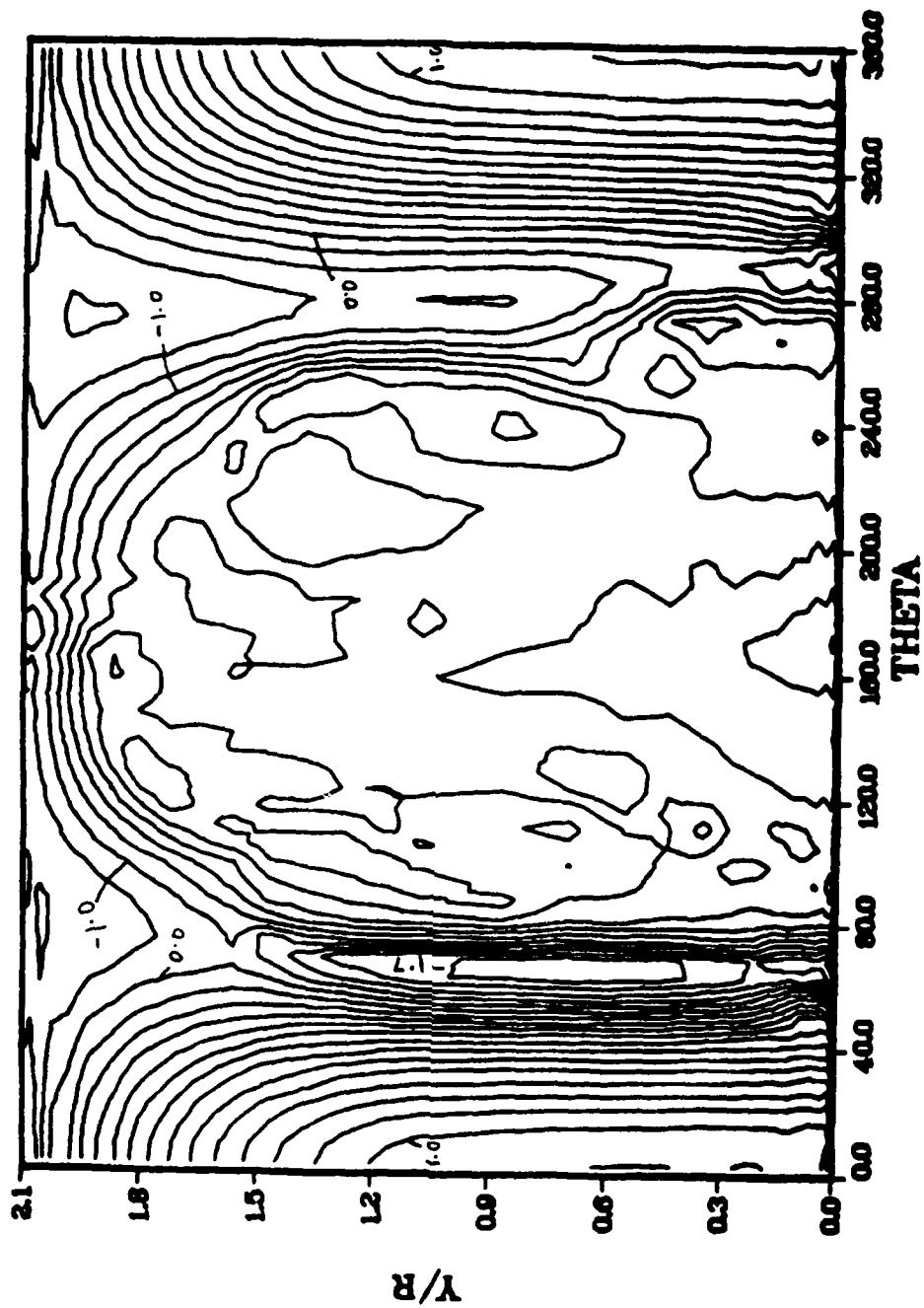
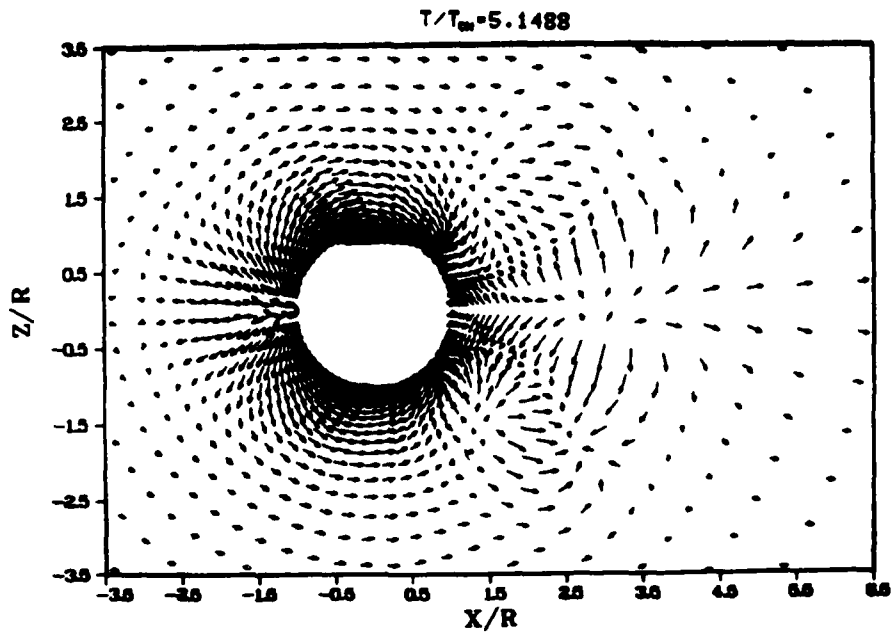


Figure 7. Instantaneous Pressure Distribution Contours Around the Turret.

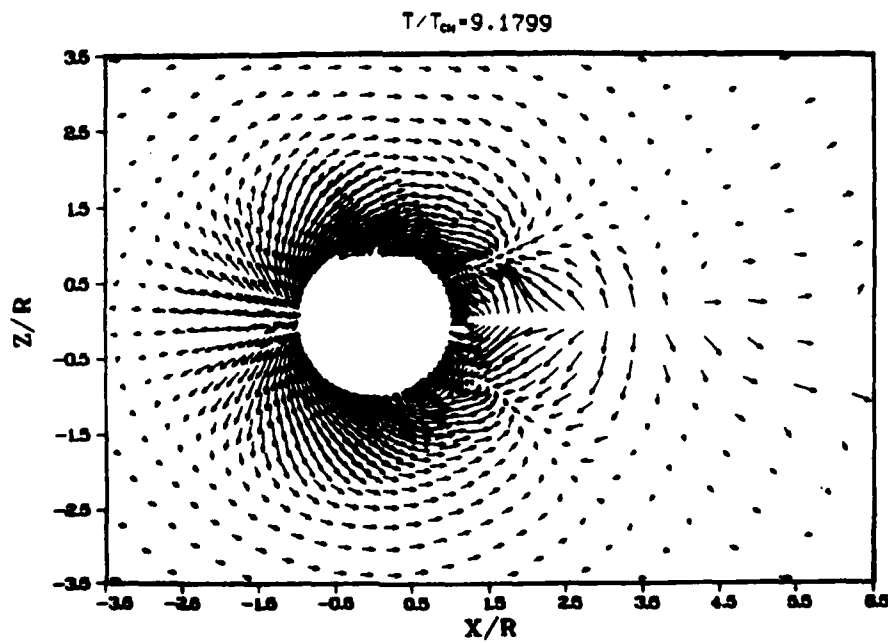
be observed at the turret window spread over 10° azimuth angles extending from slightly above the flat surface on to the hemisphere up to 37° MPA. The low valued pressure contours are mostly confined to the rear side of the turret for the azimuth angles 80° to 300° . At the turret top, the averaged computed value is -1.27 which is lower than the experimental value -1.0 . It may be recalled that the turret top is in the vicinity of 60 clustered mesh points, none of which is at the top. Our pressure coefficient value is the mean of the values at all these points. This difference may be attributed to the grid point arrangement and the improvement in this direction is one of our future goals.

A significant insight into the separated flow is offered by the limiting streamline patterns, which are, in the limiting case, the skin friction lines on the flat surface around the turret. In Figure 8, we present a sequential development of such lines that agree, at a particular instant of time, qualitatively to the work of Sedney and Kitchens^[1]. The primary separation line located at twice the turret radius upstream of the forward stagnation point and the attachment lines are quite clear and distinct. However, the secondary separation, appearing on and off near the primary separation line during the process of computation are difficult to detect. These lines merge into the primary separation line, very close to the plane of symmetry indicating that it lifts off the surface very quickly. This observation will be further confirmed when we discuss the flow field in the cross-sectional plane. The primary separation line that encircles the turret front and extends downstream in the asymmetric plane finally becomes a leg of the horseshoe vortex.

The asymmetry in the plane induced by the turret window contains some spectacular features in the downstream direction. The vortical motion in the near wake is produced by the adverse pressure gradient at this separation point and rear turret window edge. These separation points on the surface together with rear stagnation point qualify for the half saddle point (Hunt, et al.^[7]).

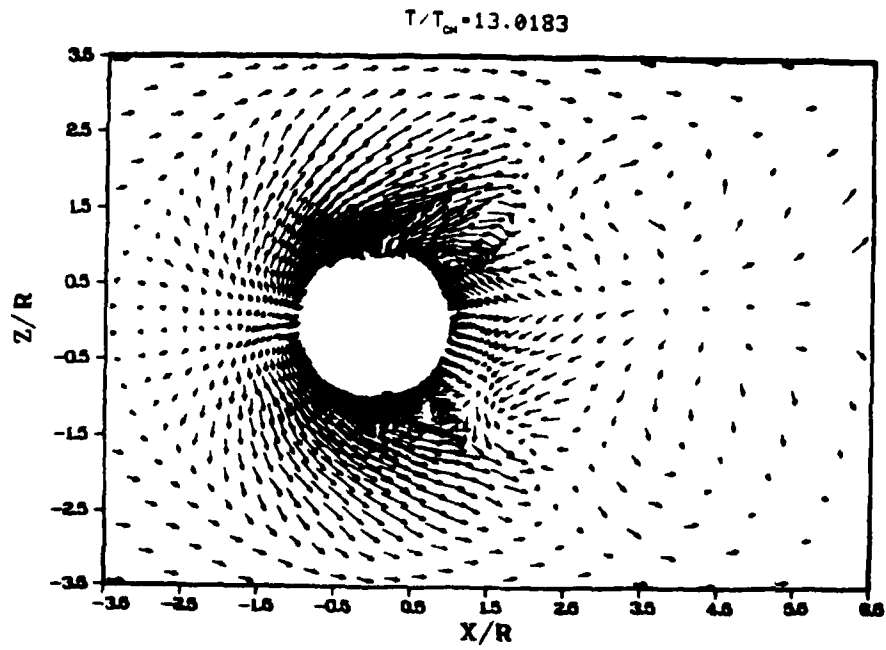


(a) $T/T_{CH} = 5.1488$

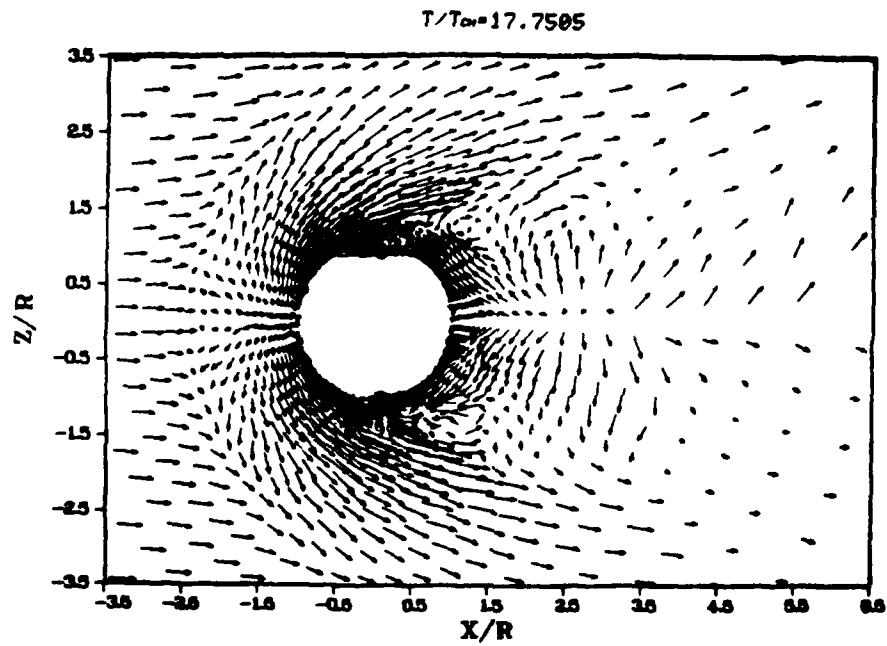


(b) $T/T_{CH} = 9.1799$

Figure 8. Instantaneous Limiting Streamline Pattern on the Flat Surface at Different Times.



(c) $T/T_{CH} = 13.0183$



$T/T_{CH} = 17.7505$

Figure 8. (Concluded) Instantaneous Limiting Streamline Pattern on the Flat Surface at Different Times.

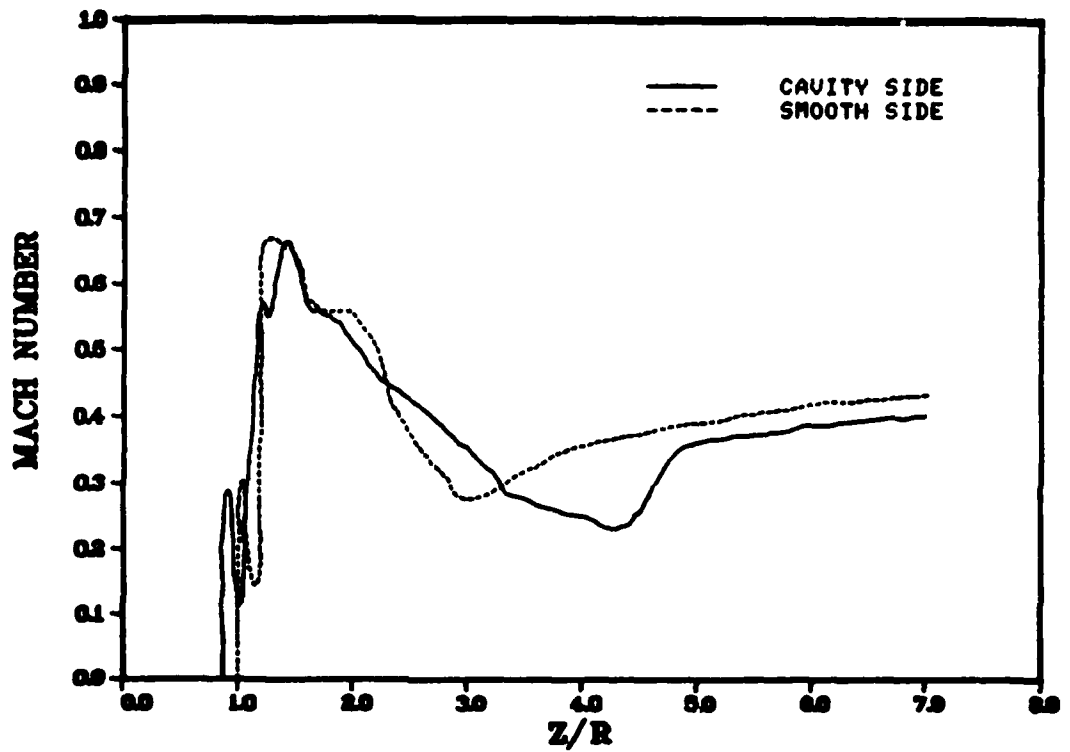
The turret window introduces an additional node and saddle point close to the surface. Accounting for the node of separation in the downstream direction, saddle point at the plane of symmetry at the primary separation, and regrouping them, the following topological rule for streamlines on a two-dimensional plane cutting the three-dimensional body is satisfied^[6].

$$(\Sigma_N + \frac{1}{2} \Sigma_N') - (\Sigma_S + \frac{1}{2} \Sigma_S') = -1 \quad (19)$$

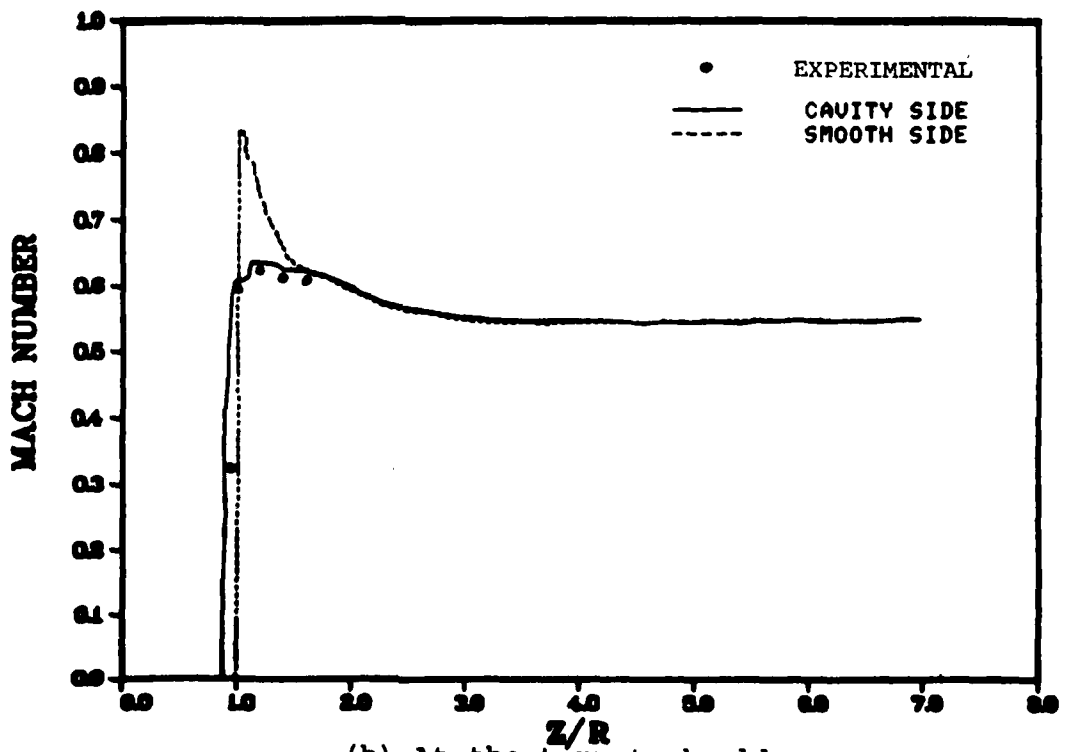
where Σ_N is the sum of the nodes and Σ_S is the sum of the saddle points. This confirmation provides a sound reasoning for coupling the analytical, experimental, and computational studies.

The asymmetry in the flow is further exemplified in Figure 9, showing the local Mach number distribution for the azimuth angle of 90° (cavity side) and 270° (smooth side). Close to the flat plate (Figure 9a), the cavity side records lower Mach number. The recovery is only 77% of the free stream value at the outer boundary which is less than 5 percent of its value at the smooth side outer boundary. This may be associated with the strong vortical flow near the rear edge of turret window and the dominant viscous effects. An altogether different situation is observed at the turret shoulder (Figure 9b), where the Mach number attains its peak values of 0.83 and 0.62, very close to the body and asymptotically approaches the free stream value within 1.5 turret radii. The experimental data^[17,18] also endorses these values.

In Figure 10 we present the RMS density fluctuations, normalized by free stream density for the azimuth angle 90°. Each curve represents the density fluctuations, at a fixed turret height, along a normal direction. The peak value, 0.0405, happens to be at the turret window base. As we move upwards, this peak value shows a decreasing trend and then oscillates between 0.009 and 0.003 (Figure 11). The corresponding peak value^[11] (experimental) is 0.034, 19 percent lower than our computed result. This experimental value was deduced from the hot wire data using an empirical



(a) Close to the flat surface.



(b) At the turret shoulder.

Figure 9. Mach Number Distribution.

- EXPERIMENTAL
- COMPUTED
- ① $\frac{Y}{R} = 0.4479$
- ② $\frac{Y}{R} = 0.5620$
- ③ $\frac{Y}{R} = 0.8712$
- ④ $\frac{Y}{R} = 1.1794$
- ⑤ $\frac{Y}{R} = 1.649$

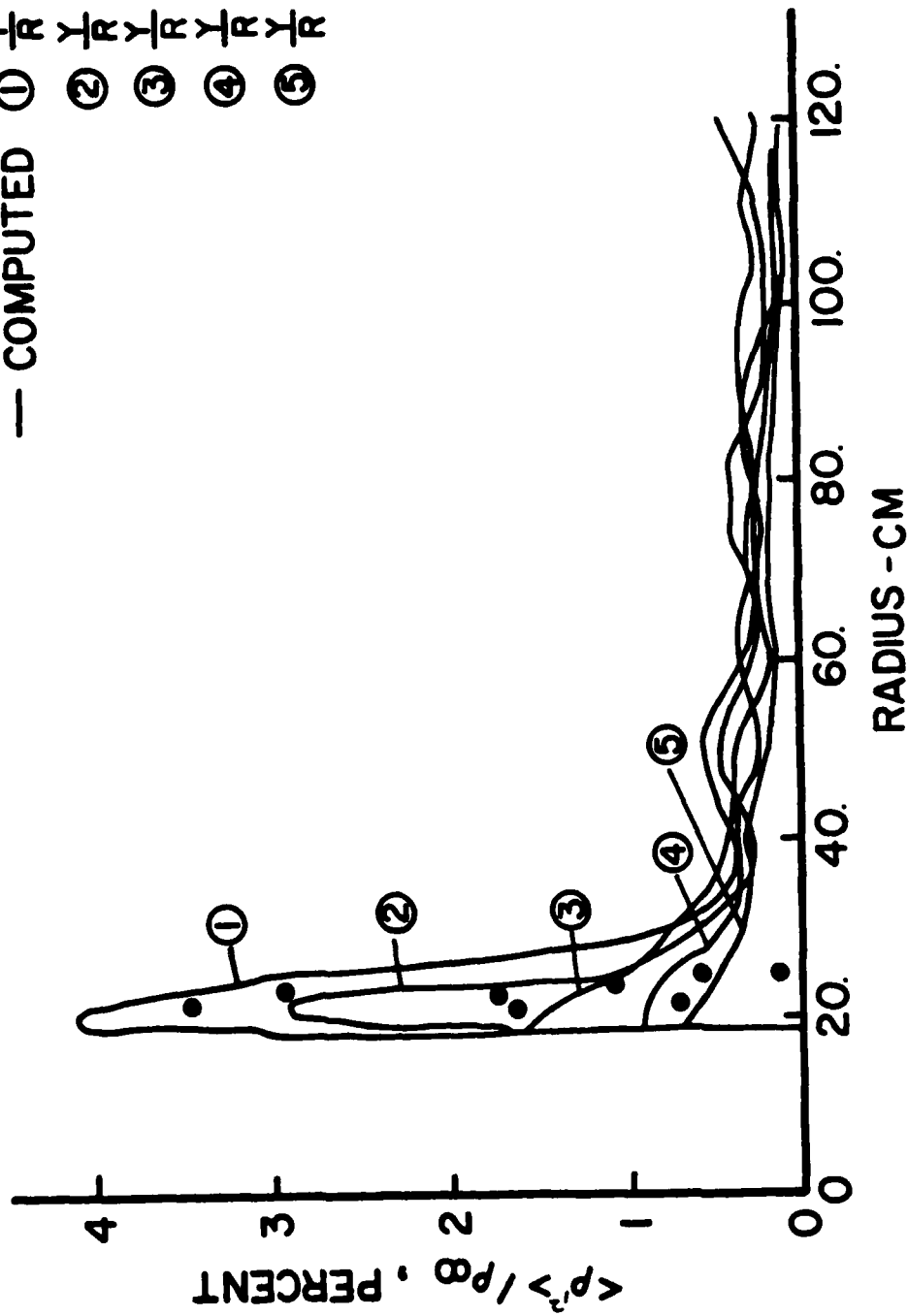


Figure 10. RMS Density Fluctuations for the 90° Azimuth Angle.

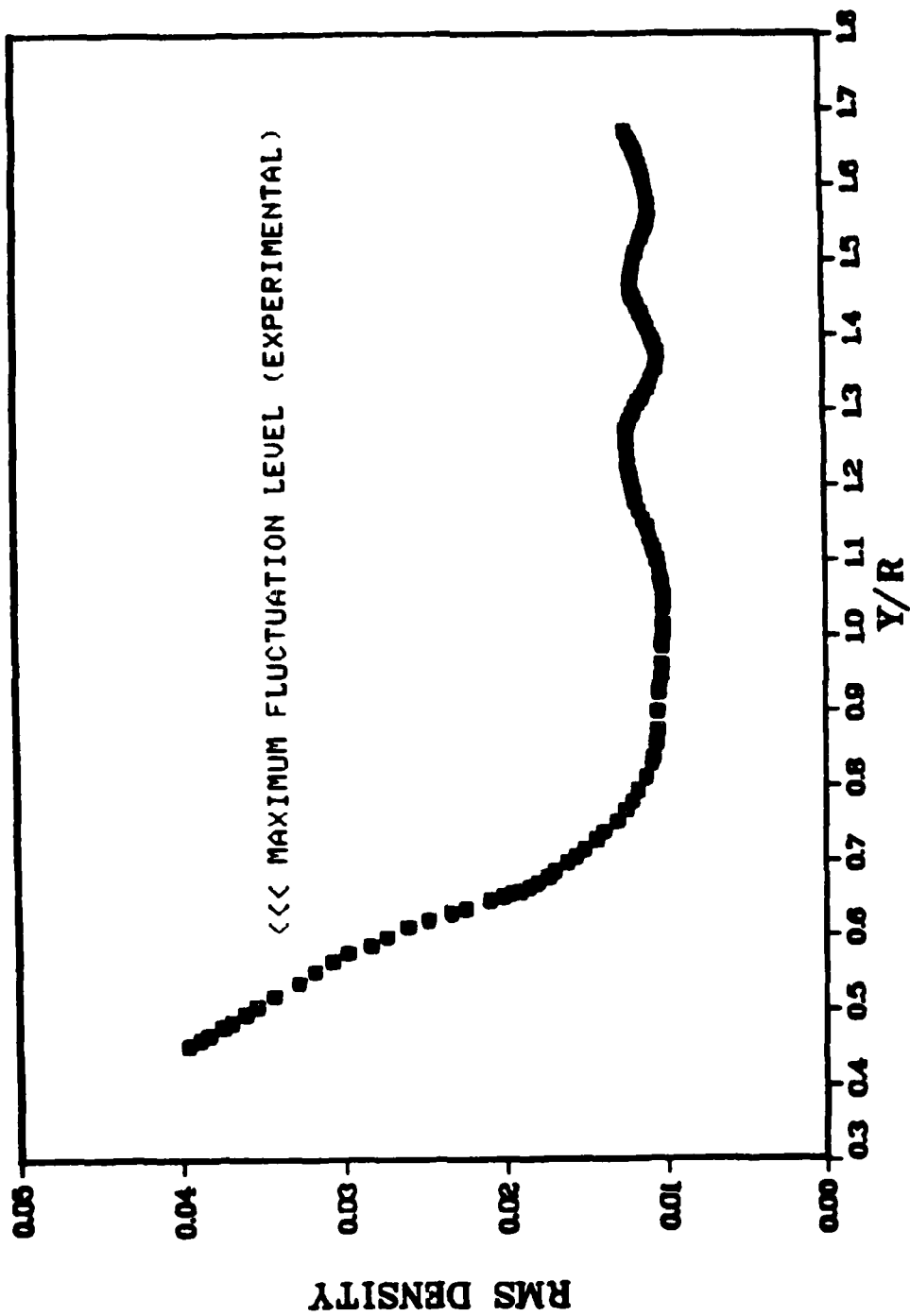
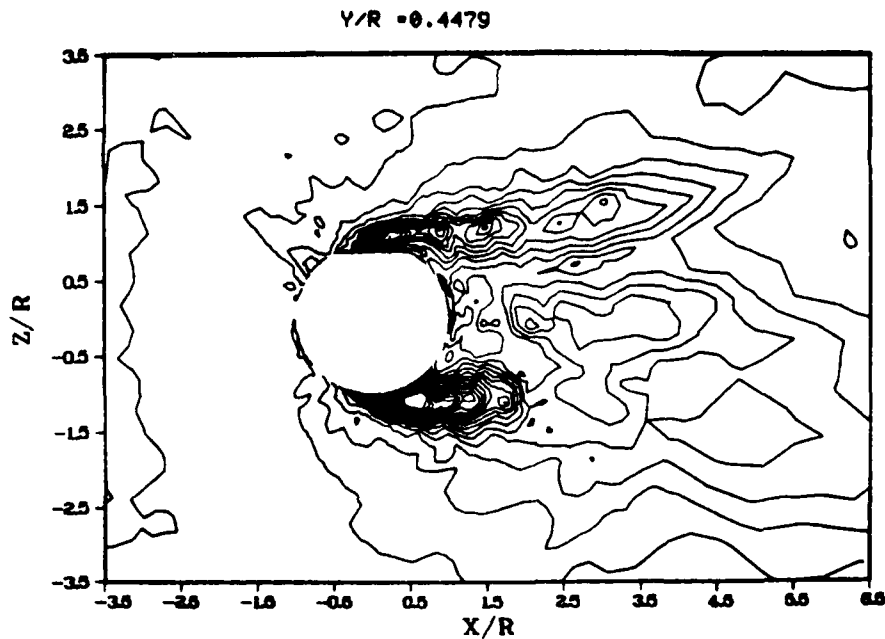


Figure 11. Peak RMS Density Fluctuation at Various Turret Window Heights.

relation and ignoring the higher order pressure fluctuations. The far field fluctuations, which are small, might not be of major concern, but in the near field the turret base is most sensitive to such fluctuations. This fact is further elaborated in Figure 12, giving RMS density fluctuation contours at the base, middle, and top of the turret window. It is interesting to observe that these fluctuations are grouped at two different locations and the peak value, 0.073, occurs at AZA = 246°. These fluctuations of high intensity slip off towards the downstream direction and cluster between AZA = 100° and 210° with a peak value of 0.04 at AZA = 190°. The density in the upstream direction remains almost invariant and does not give rise to any substantial fluctuations.

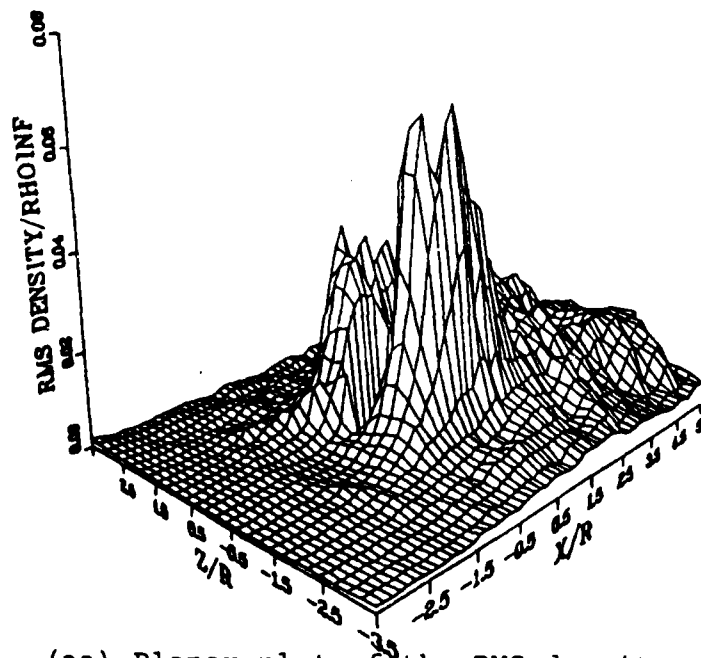
Figure 13, 14, 15 give a glimpse of the flow field structure in the cross-sectional plane (azimuth angle 0° - 180°) of the computational domain. It presents the instantaneous velocity field, Mach number, and density contours in a sequential manner. The significant upstream influence is confined close to the flat plate up to 2.5 times the turret radius. The velocity field is suggestive of an interesting feature: along the front stagnation line on the cylindrical surface, the flow is almost divided into two parts. At $\frac{Y}{R} = 0.3543$, the contribution of the axial velocity component is negligible compared to the tangential and normal components. The accelerating flow at the hemispherical dome, with a maximum Mach number of 0.87 at 72° MPA upstream, is separated at 47° MPA in the downstream direction. The reverse flow in the near wake region and at the turret shoulder and their time dependent variation provide the mechanism for vortex shedding and the relative movement of reattachment point.

Complementary to this cross-sectional plane, the flow field distribution in the plane parallel to the flat plate offers a qualitative comparison to flow past a cylinder. In this plane, up to the turret shoulder, the fluid phenomenon shows a similar trend. As a typical example, the velocity field distribution, Mach number, and density contours are presented at two different



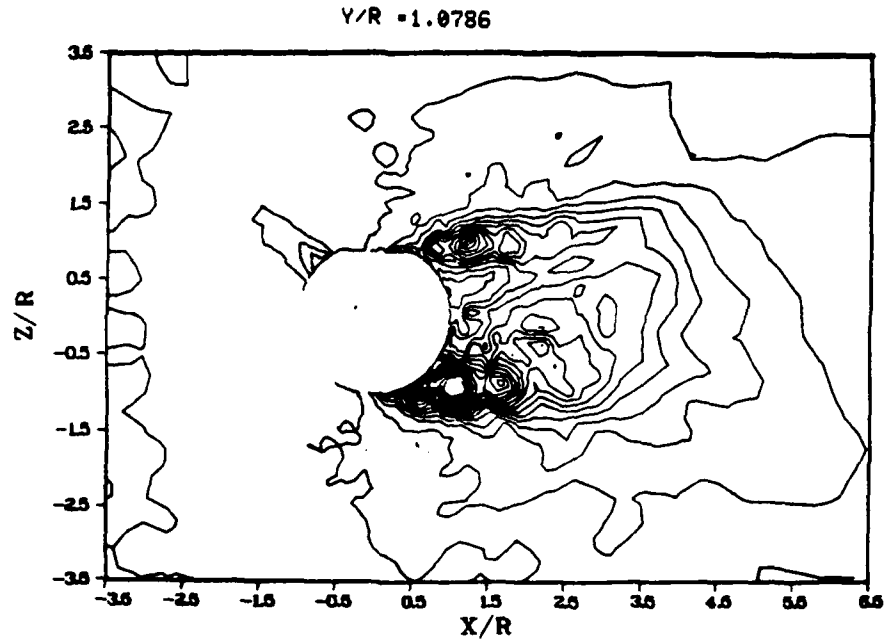
(a) Contours of the RMS density fluctuations for $Y/R = 0.4479$.

RMS DENSITY TRT WINDOW BASE



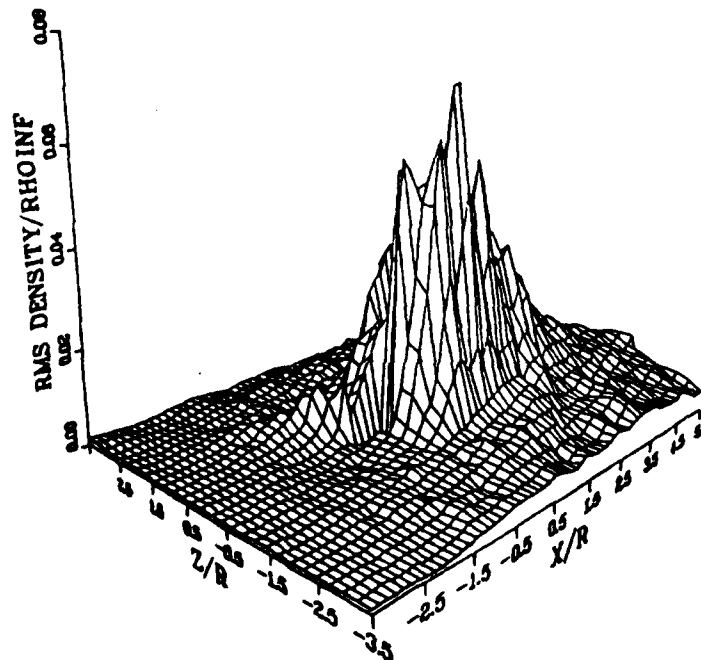
(aa) Planar plot of the RMS density fluctuations for $Y/R = 0.4479$.

Figure 12. RMS Density Fluctuation Contours and Planar Plots.



(b) Contours of the RMS density fluctuations for $Y/R = 1.0786$.

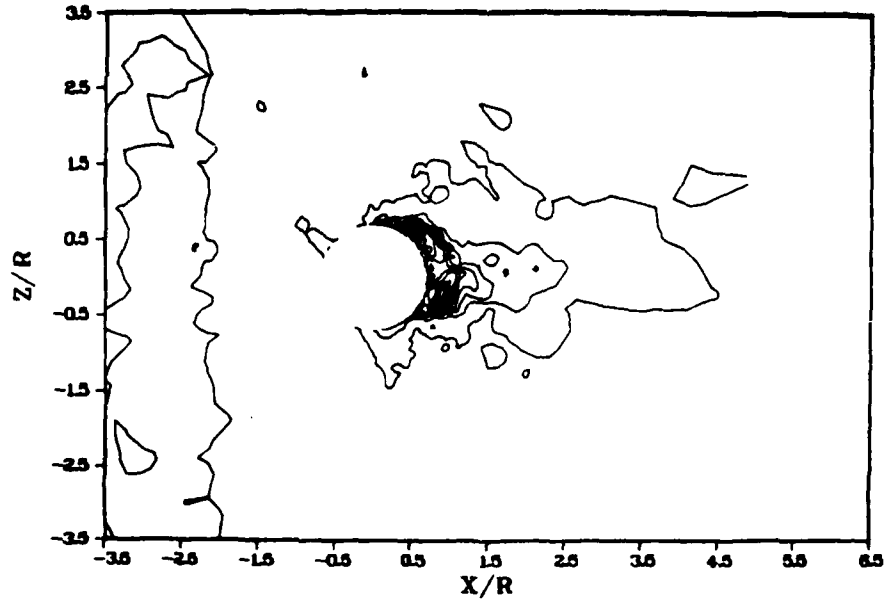
RMS DENSITY TRT WINDOW CENTER



(bb) Planar plot of the RMS density fluctuations for $Y/R = 1.0786$.

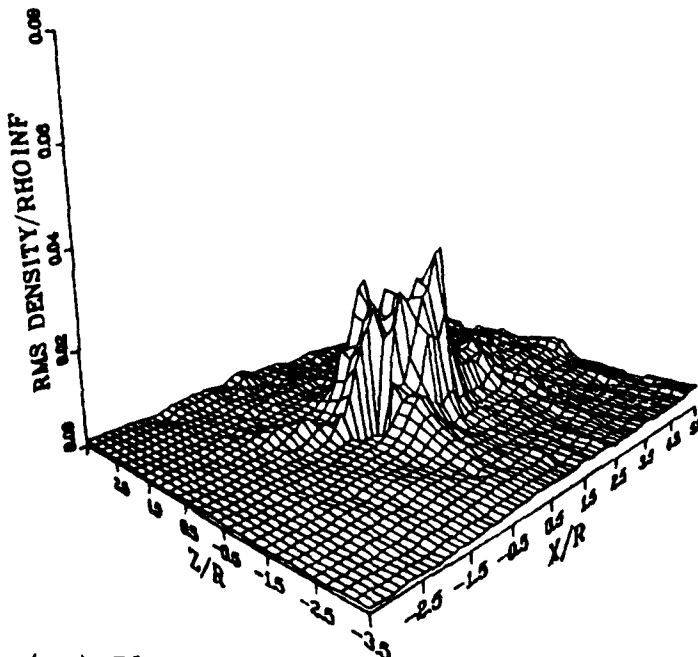
Figure 12. (Continued) RMS Density Fluctuation Contours and Planar Plots.

Y/R = 1.6490



(c) Contours of the RMS density fluctuations for Y/R = 1.6490.

RMS DENSITY TRT WINDOW TOP



(cc) Planar plot of the RMS density fluctuations for Y/R = 1.6490.

Figure 12. (Concluded) RMS Density Fluctuation Contours and Planar Plots.

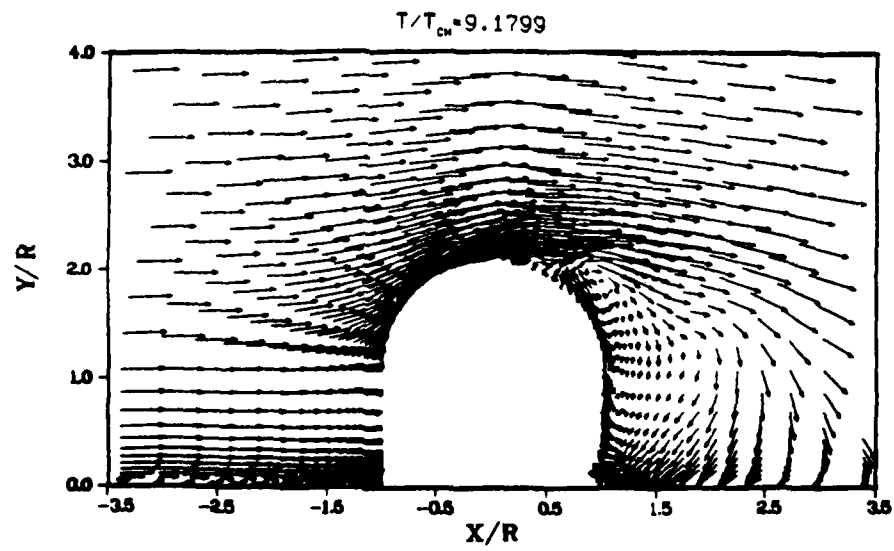
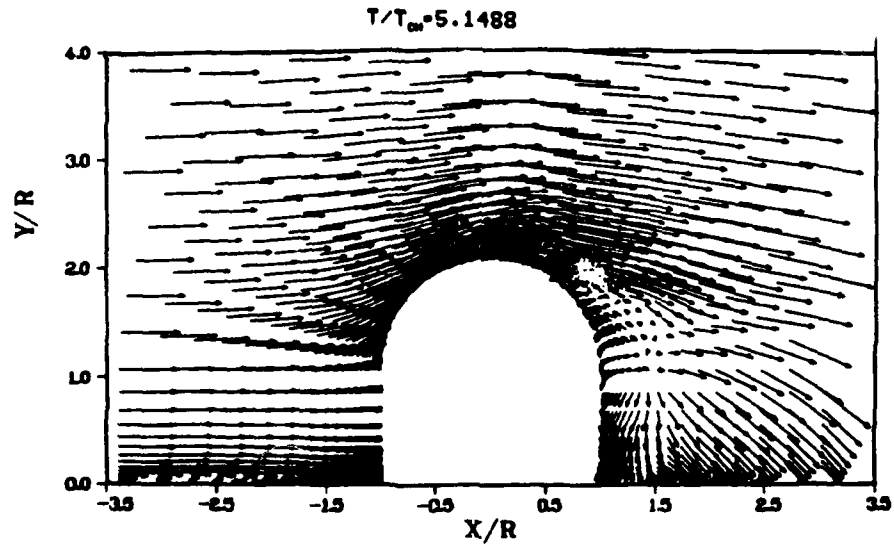
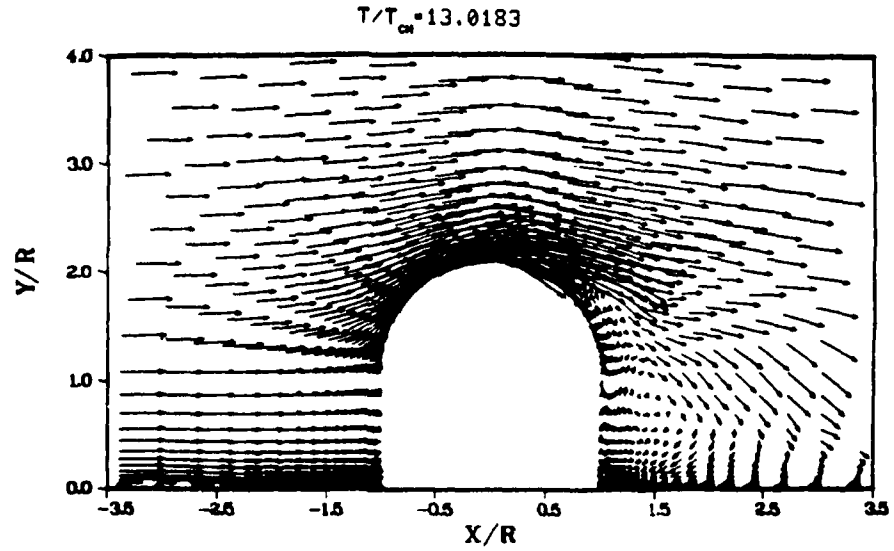
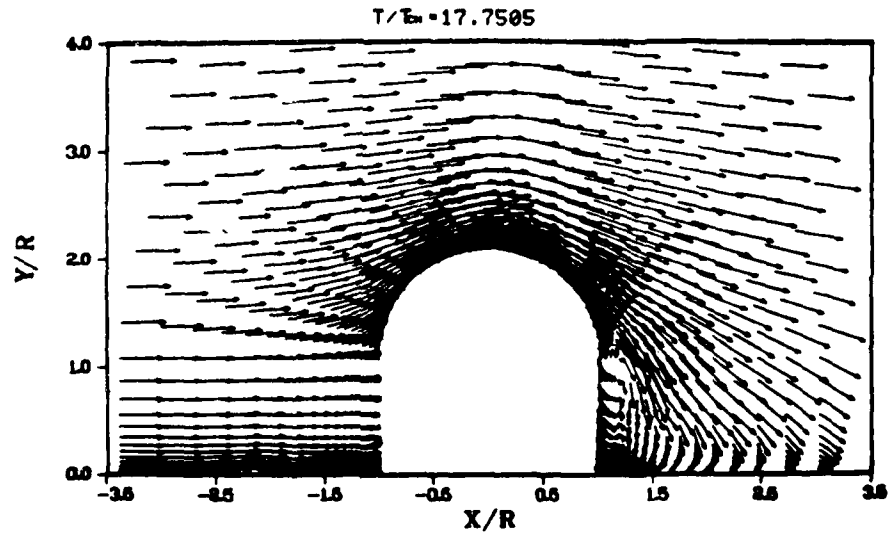


Figure 13. Velocity Field in the Cross-sectional Plane at Different Times.

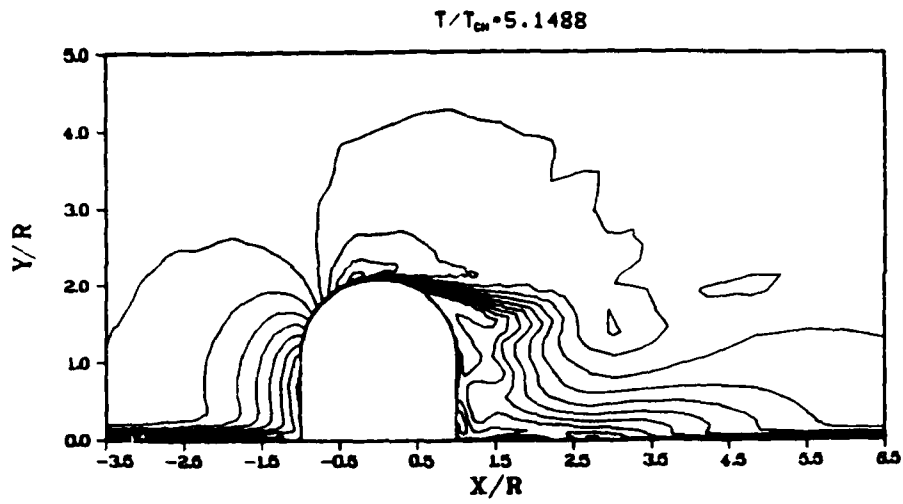


(c) $T/T_{CH} = 13.0183$

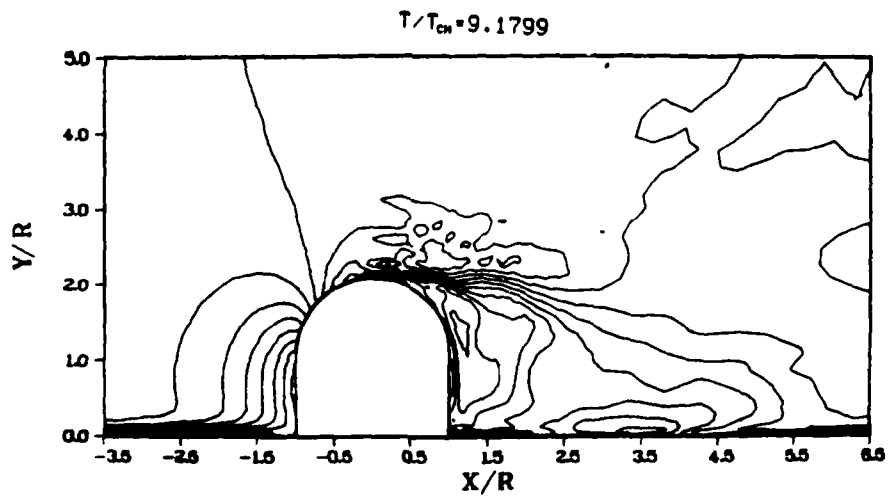


(d) $T/T_{CH} = 17.7505$

Figure 13. (Concluded) Velocity Field in the Cross-sectional Plane at Different Times.



(a) $T/T_{CH} = 5.1488$



(b) $T/T_{CH} = 9.1799$

Figure 14. Mach Number Contours in the Cross-sectional Plane at Different Times.

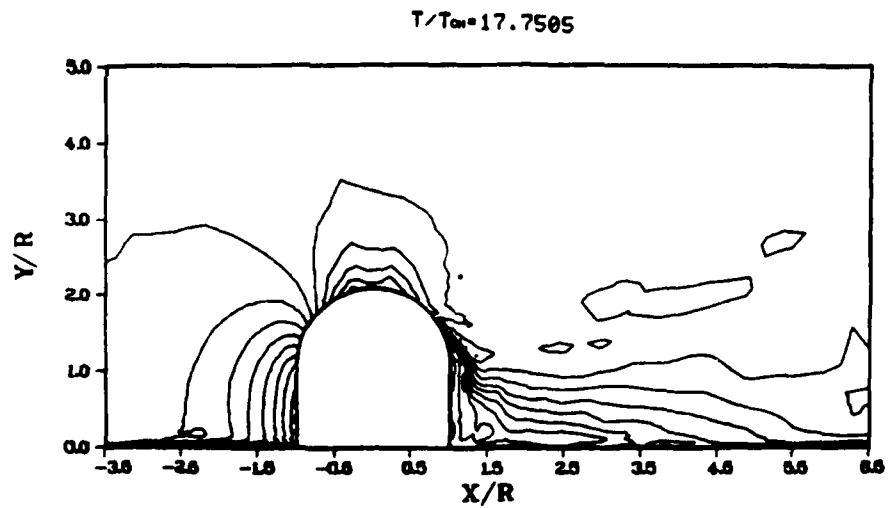
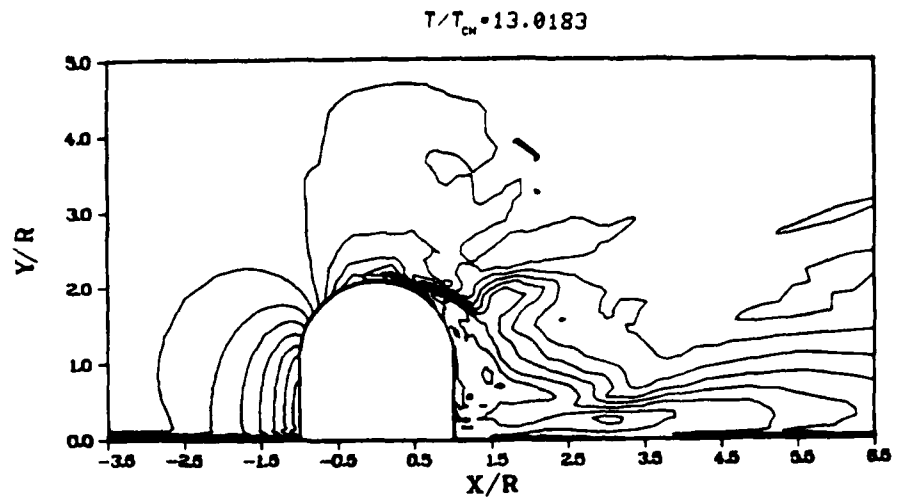


Figure 14. (Concluded) Mach Number Contours in the Cross-sectional Plane at Different Times.

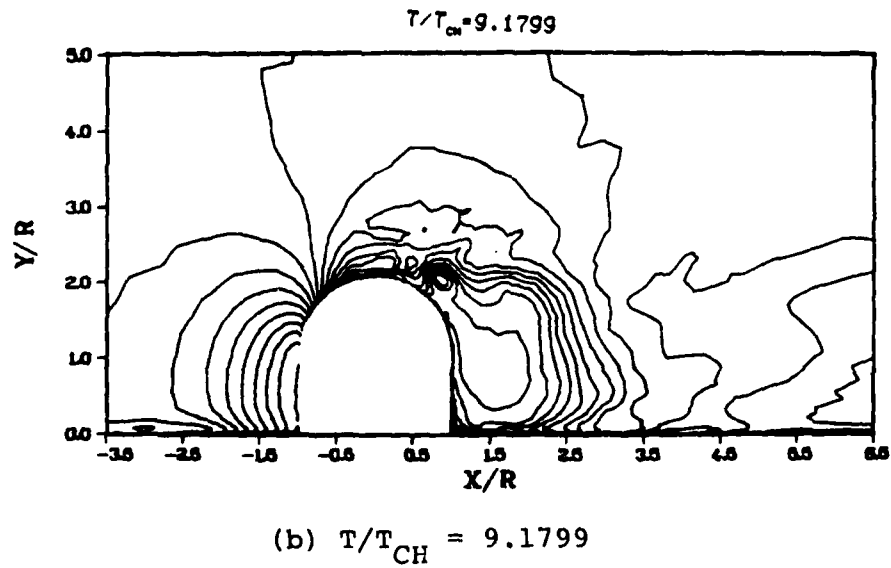
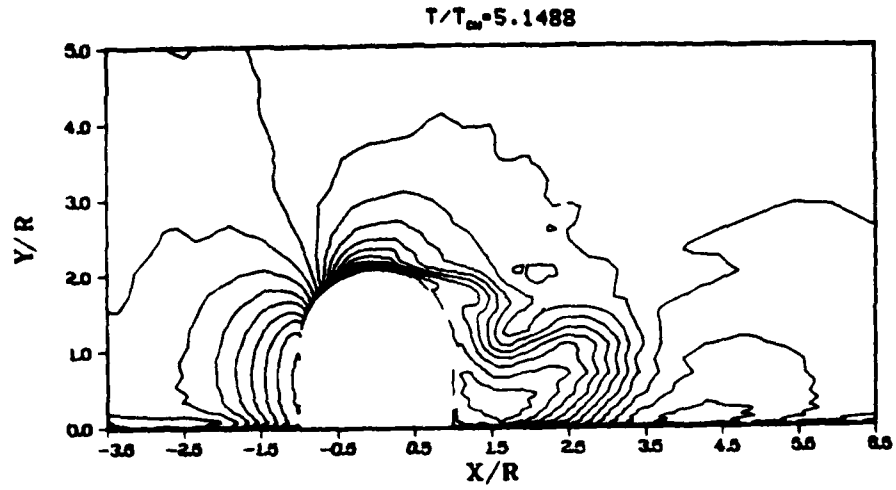


Figure 15. Density Contours in the Cross-sectional Plane at Different Times.

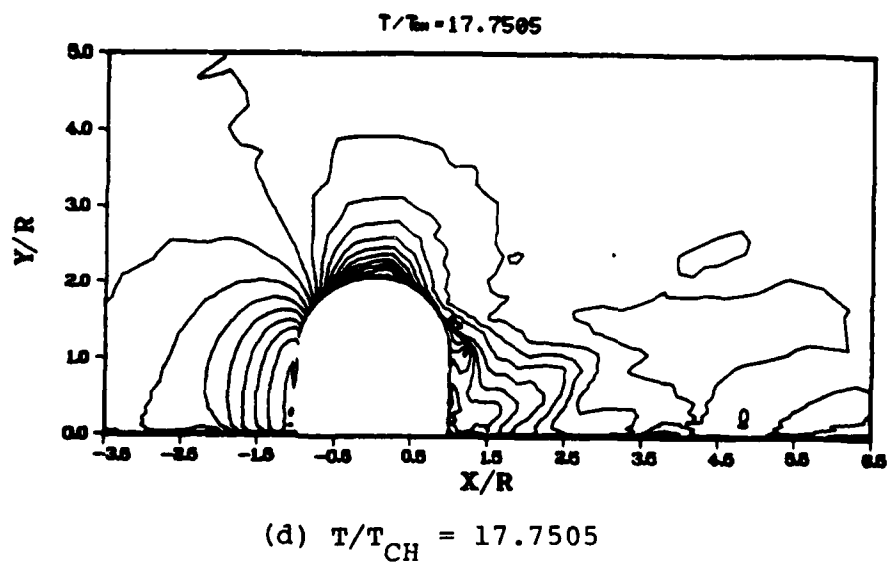
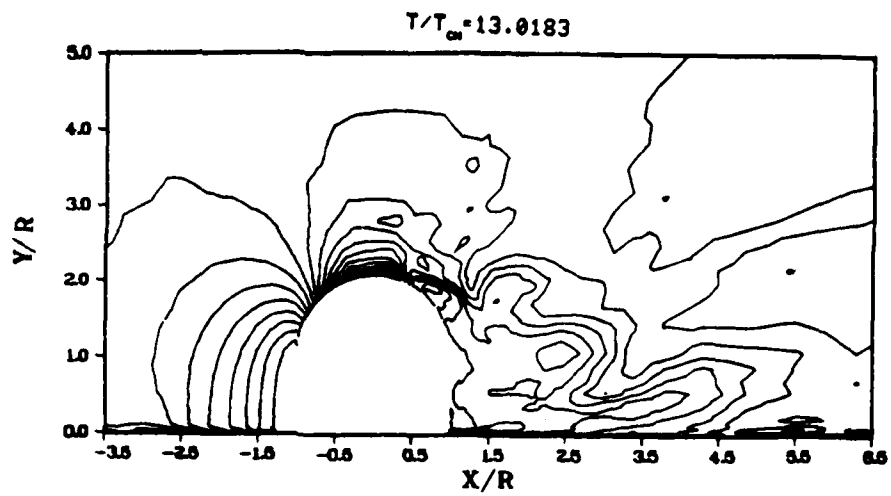


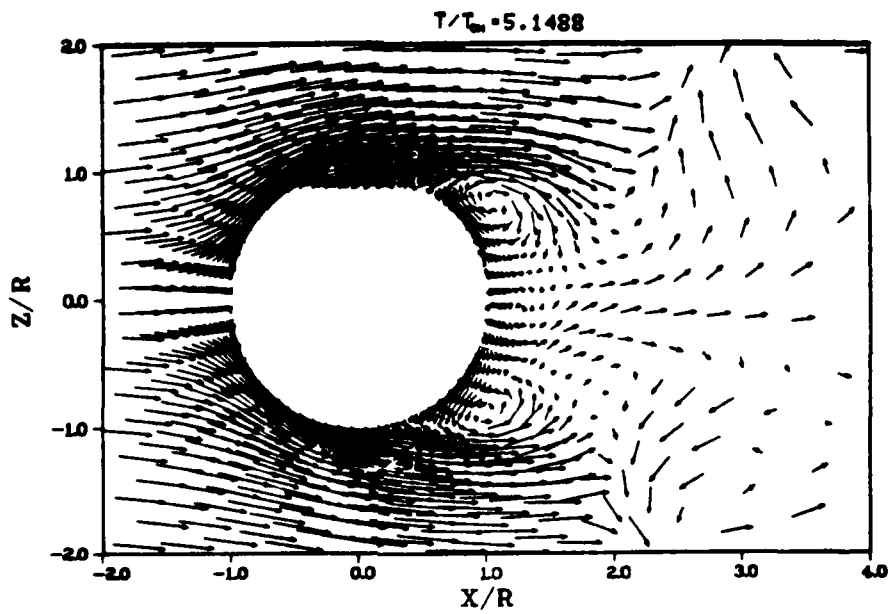
Figure 15. (Concluded) Density Contours in the Cross-sectional Plane at Different Times.

locations (Figures 16 through 18, at $\frac{Y}{R} = 0.3543$ and Figures 19 through 21, at turret shoulder). The turret window contributes an additional amplification to the process of vortex shedding in the downstream direction. At the turret shoulder, the maximum local Mach number attained was 0.93 at AZA = 63° and 0.90 at AZA = 270°. These values are much lower than that for the corresponding two-dimensional case^[10], where transition and even shock wave formation is reported. Also, the separation point has advanced further downstream towards the rear stagnation point at AZA = 99° and 243°, respectively. Even though the separation point location is a function of time, it is observed that for a particular instant of time, the locus of the separation point, the separation line, changes its course considerably along the turret height. This illuminating fact is further revealed in Figure 22.

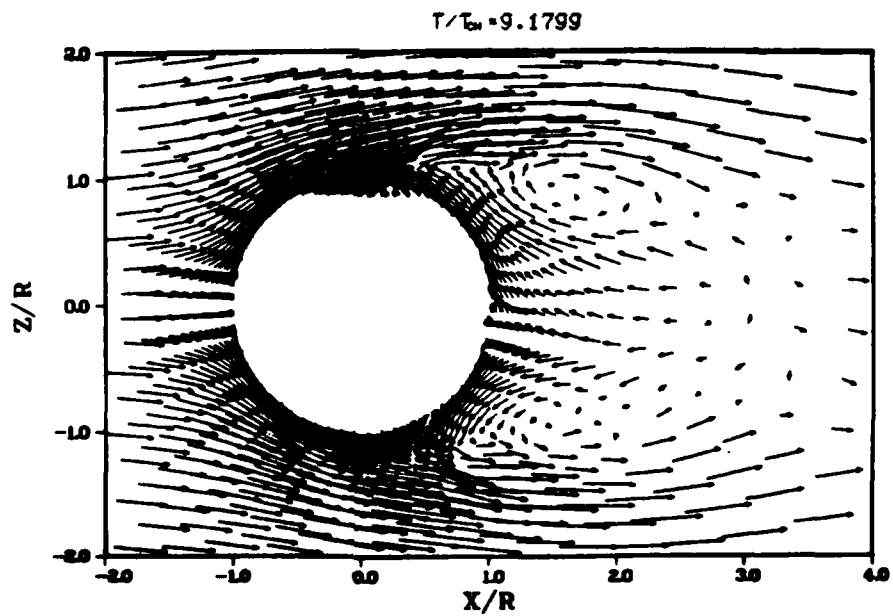
This Figure shows an instantaneous limiting streamline pattern on the turret surface. Near the stagnation point, a saddle point type singularity, a foci, node of attachment along the turret height can be easily identified. The turret window includes an additional small separation zone and, hence, introduces a node and saddle point. These singular points, together with the nodes at the forward and rearward stagnation points, give another confirmation to the topological criteria. For the skin friction lines on a three-dimensional body, B, connected simply to a plane wall, P, the sum of nodes, Σ_N and the sum of saddle points, Σ_S satisfy the following relation^[6]

$$(\Sigma_N - \Sigma_S)_{P+B} = 0. \quad (20)$$

The asymmetric separation lines start just above the foci, at the turret base, climb up towards the hemisphere and then meet at the rear stagnation line at 30° MPA. The separation effects on the turret top are mostly confined to 63° MPA. On the cylindrical surface, near the turret shoulder, the separation points show a tendency to move upstream indicating that strong three-dimensional flow exists.

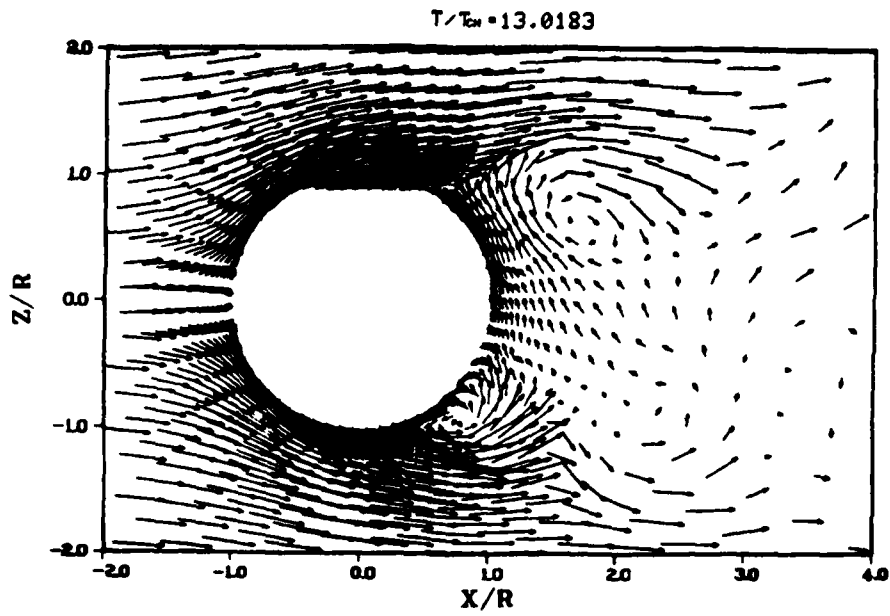


(a) $T/T_{CH} = 5.1488$

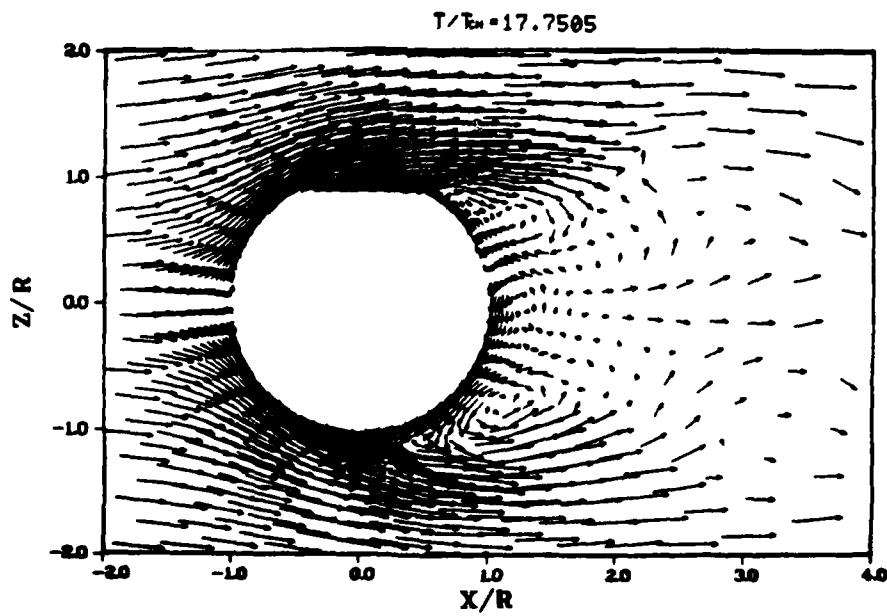


(b) $T/T_{CH} = 9.1799$

Figure 16. Velocity Field Around the Turret at $\frac{Y}{R} = 0.3543$ at Different Times.



(c) $T/T_{CH} = 13.0183$



(d) $T/T_{CH} = 17.7505$

Figure 16. (Concluded) Velocity Field Around the Turret
at $\frac{Y}{R} = 0.3543$ at Different Times.

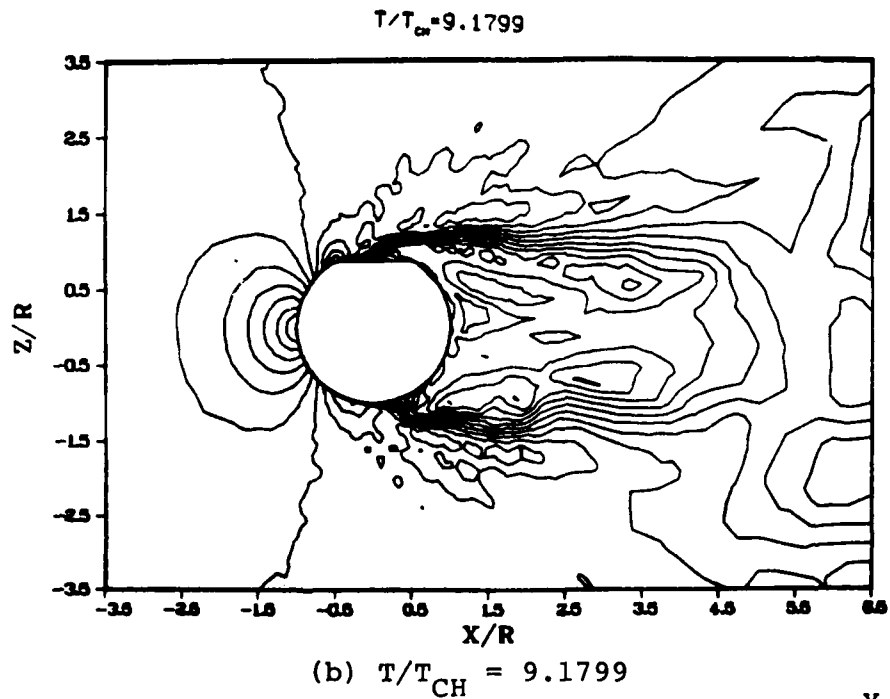
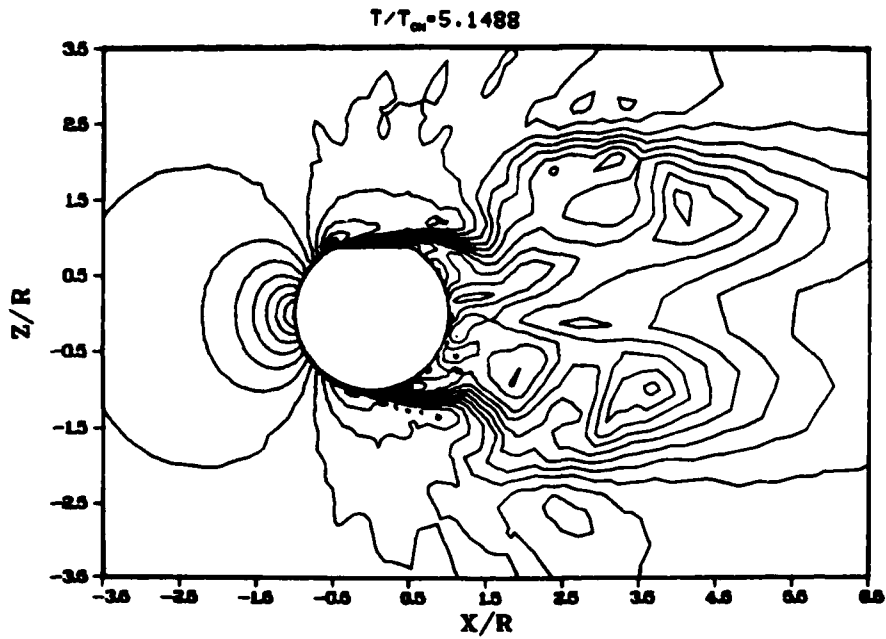
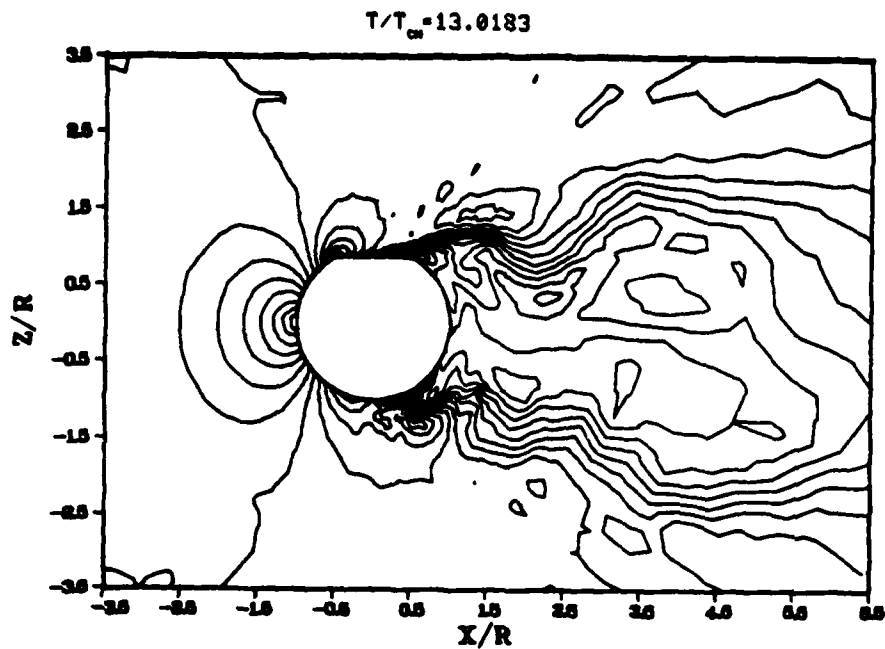
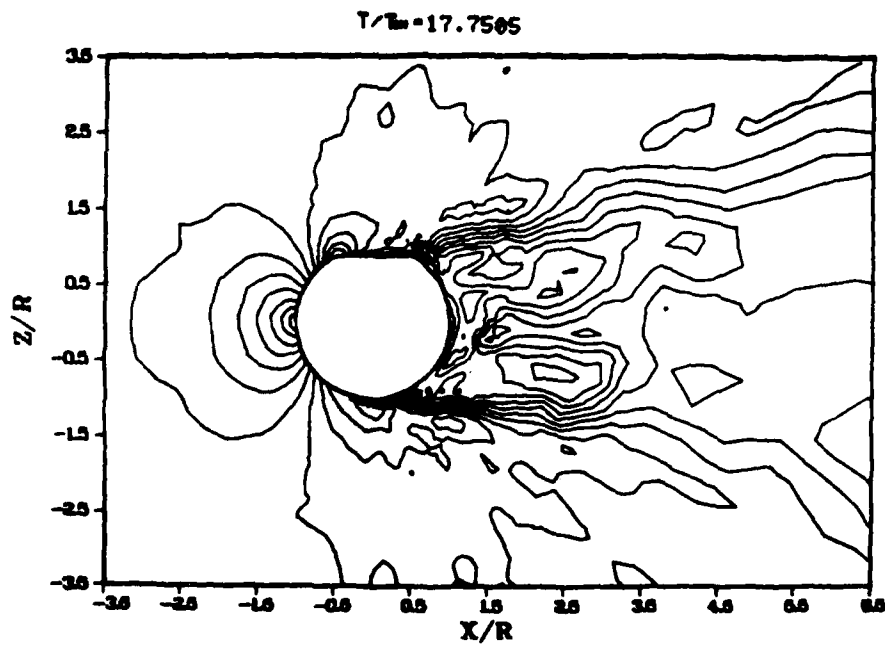


Figure 17. Mach Number Contours Around the Turret at $\frac{Y}{R} = 0.3543$ at Different Times.

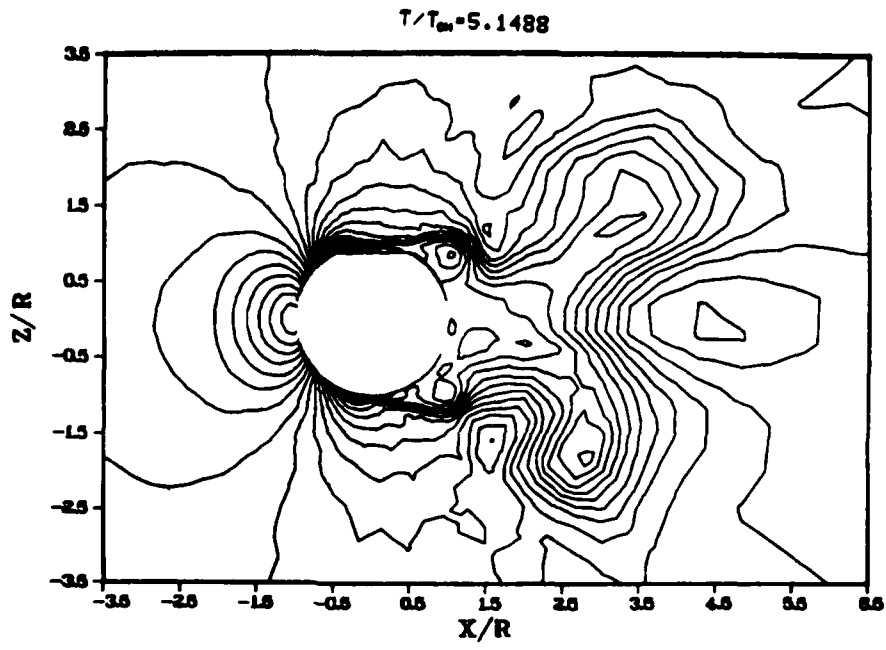


(c) $T/T_{CH} = 13.0183$

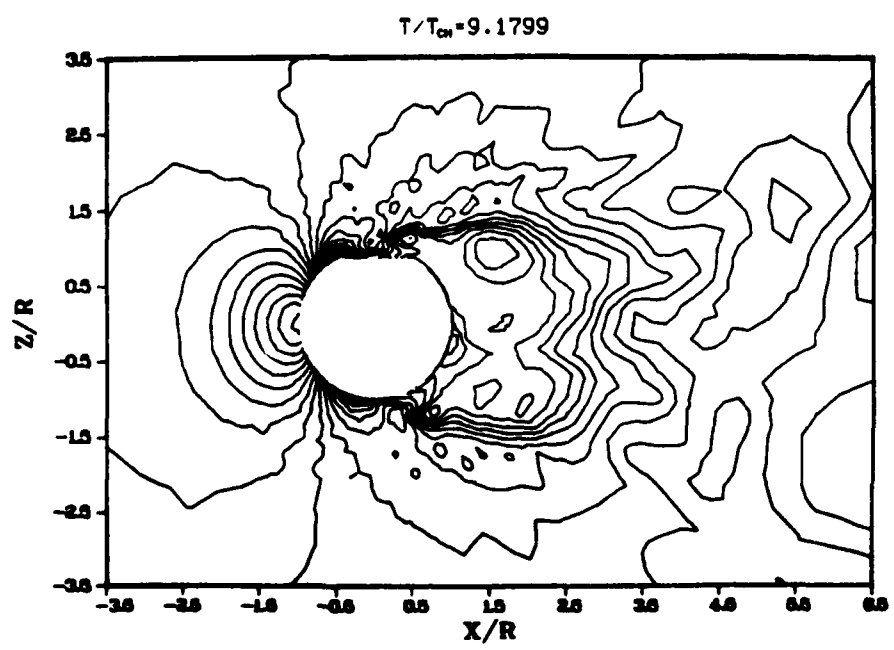


(d) $T/T_{CH} = 17.7505$

Figure 17. (Concluded) Mach Number Contours Around the Turret at $\frac{Y}{R} = 0.3543$ at Different Times.

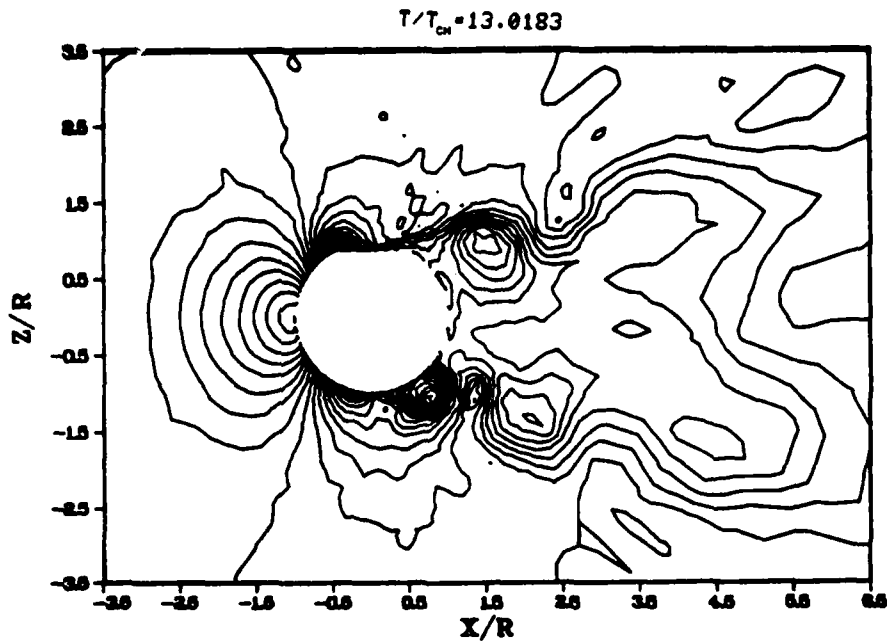


(a) $T/T_{CH} = 5.1488$

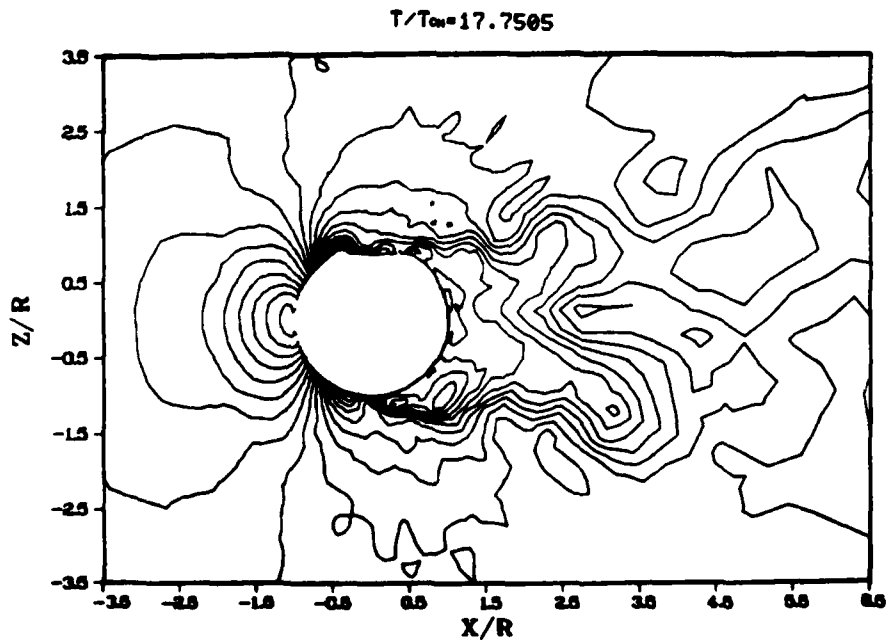


(b) $T/T_{CH} = 9.1799$

Figure 18. Density Contours Around the Turret at $\frac{Y}{R} = 0.3543$ at Different Times.



(c) $T/T_{CH} = 13.0183$



(d) $T/T_{CH} = 17.7505$

Figure 18. (Concluded) Density Contours Around the Turret at $\frac{Y}{R} = 0.3543$ at Different Times.

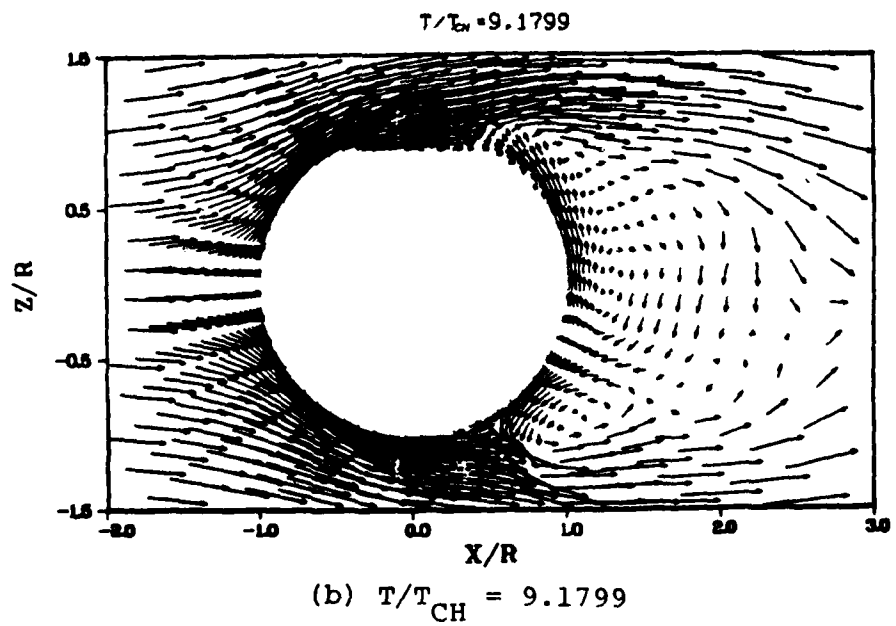
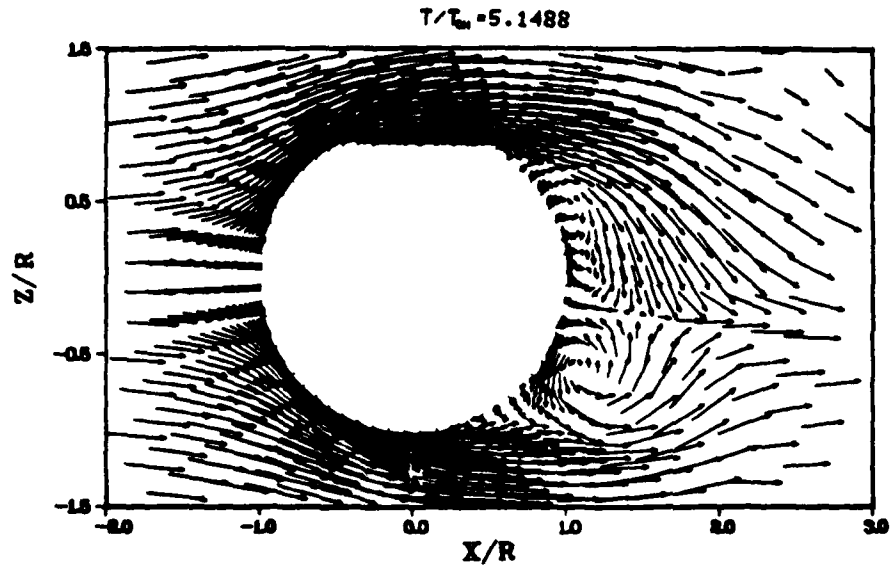
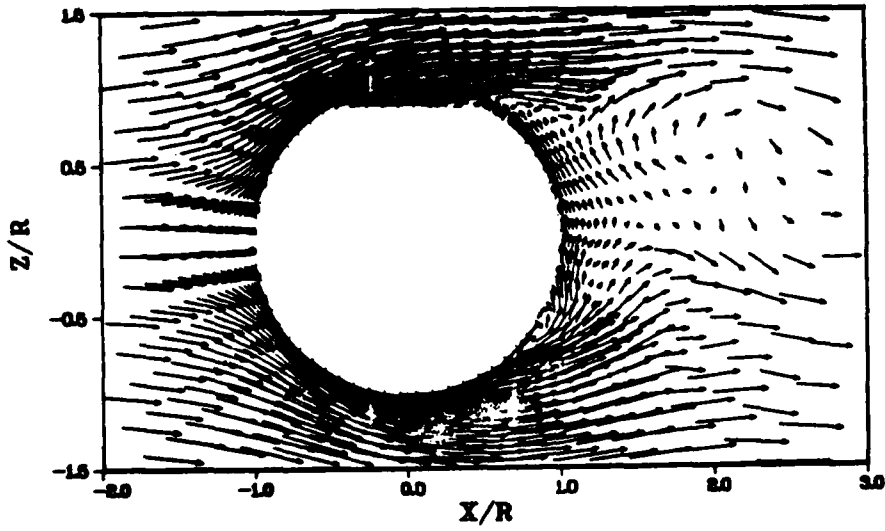


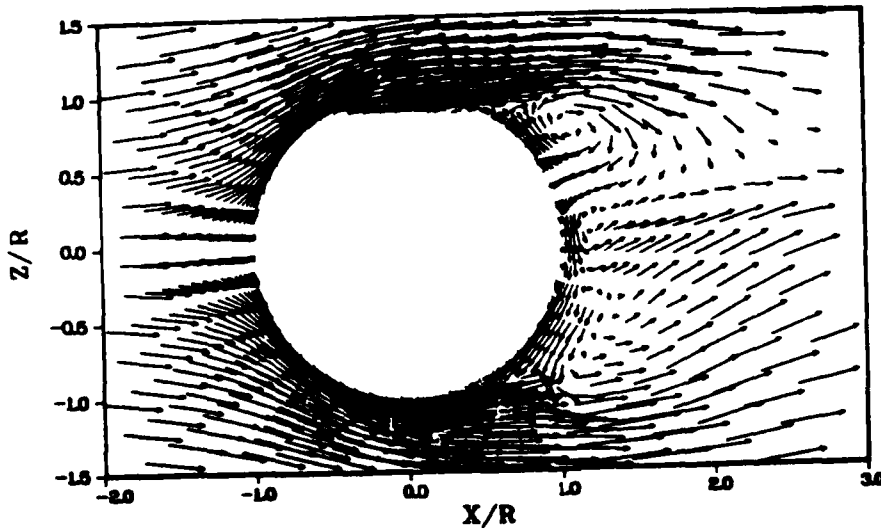
Figure 19. Velocity Field Around the Turret at Different Times.

$T/T_{CH} = 13.0183$



(c) $T/T_{CH} = 13.0183$

$T/T_{CH} = 17.7505$



(d) $T/T_{CH} = 17.7505$

Figure 19. (Concluded) Velocity Field Around the Turret at Different Times.

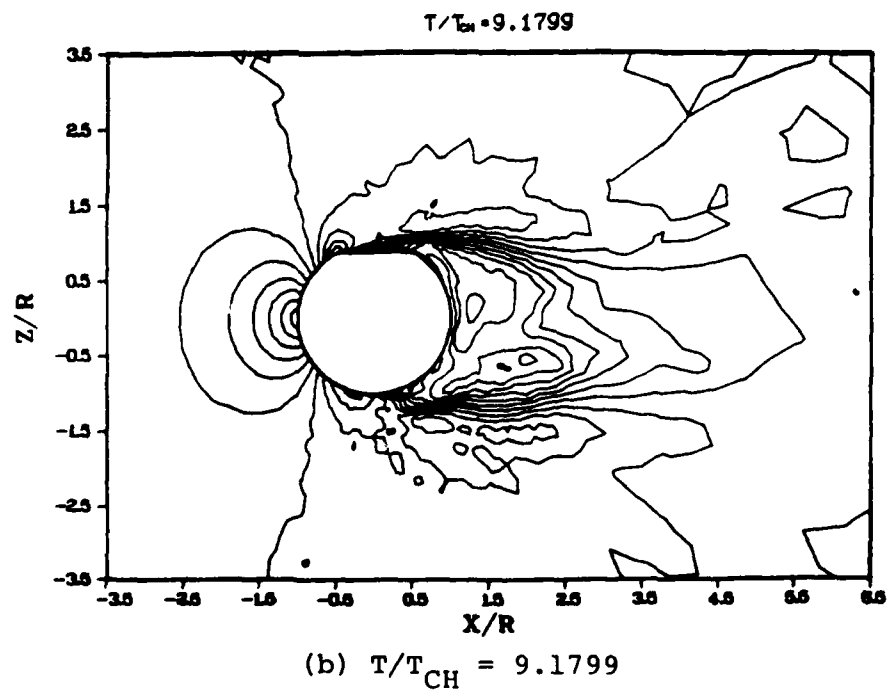
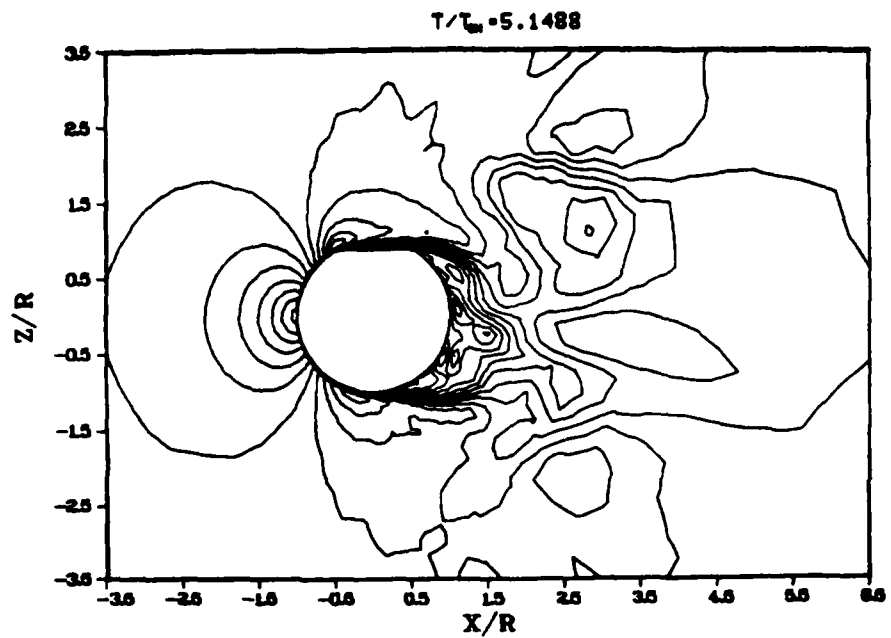
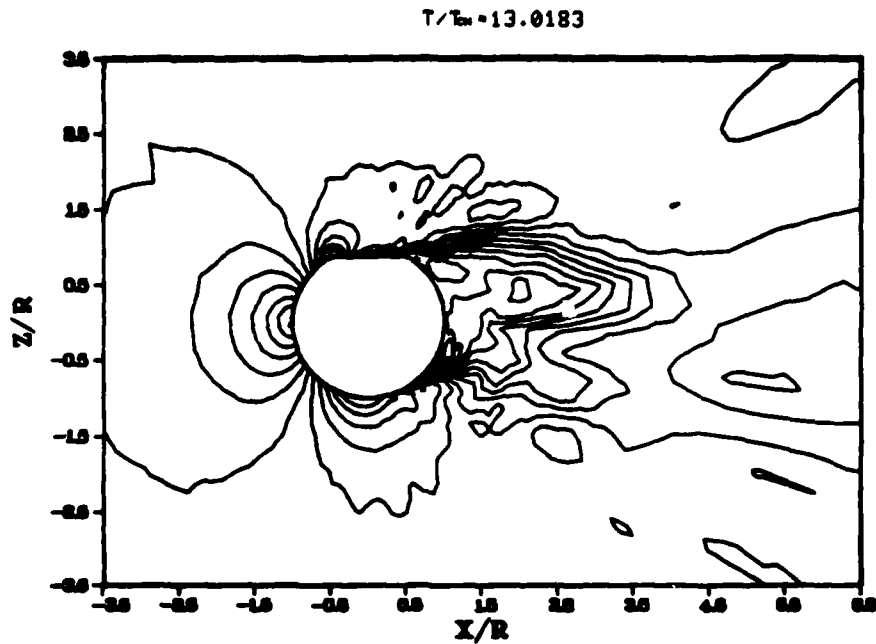
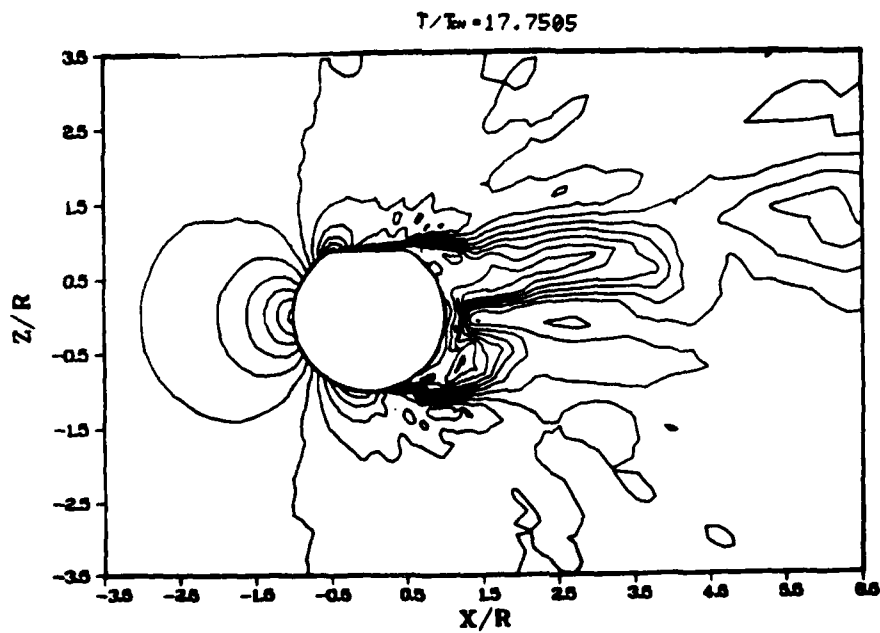


Figure 20. Mach Number Contours Around the Turret Shoulder at Different Times.

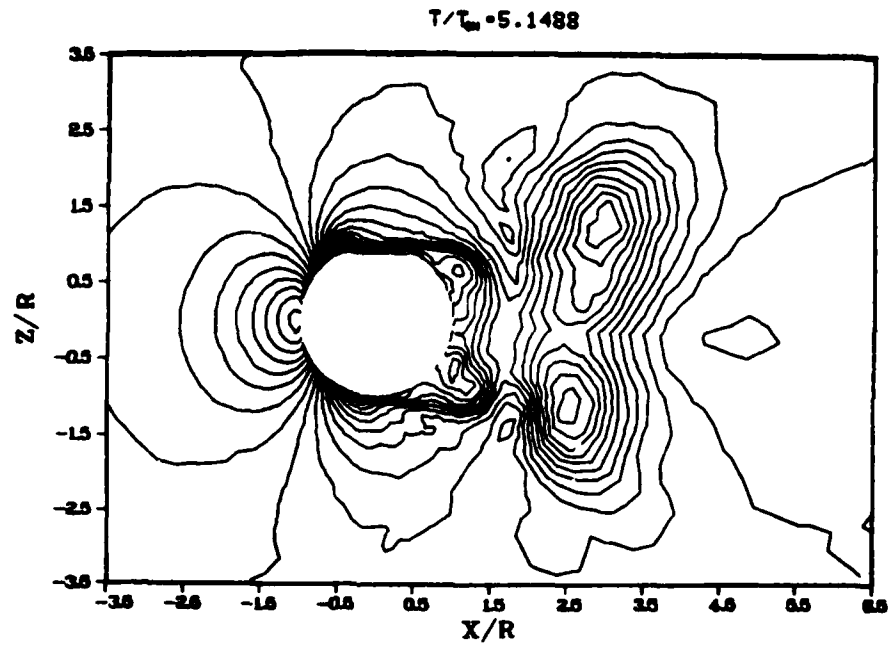


(c) $T/T_{CH} = 13.0183$

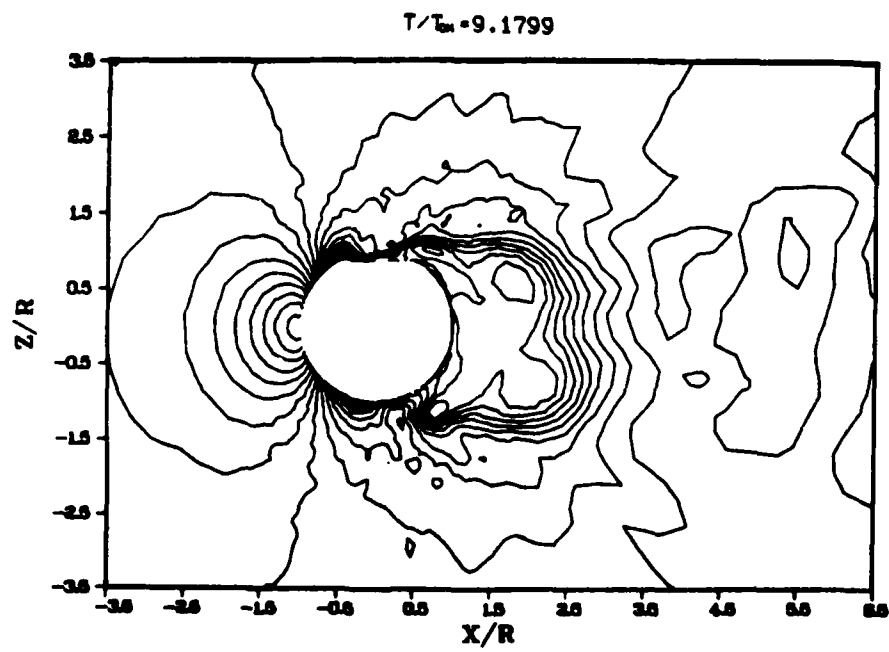


(d) $T/T_{CH} = 17.7505$

Figure 20. (Concluded) Mach Number Contours Around the Turret Shoulder at Different Times.

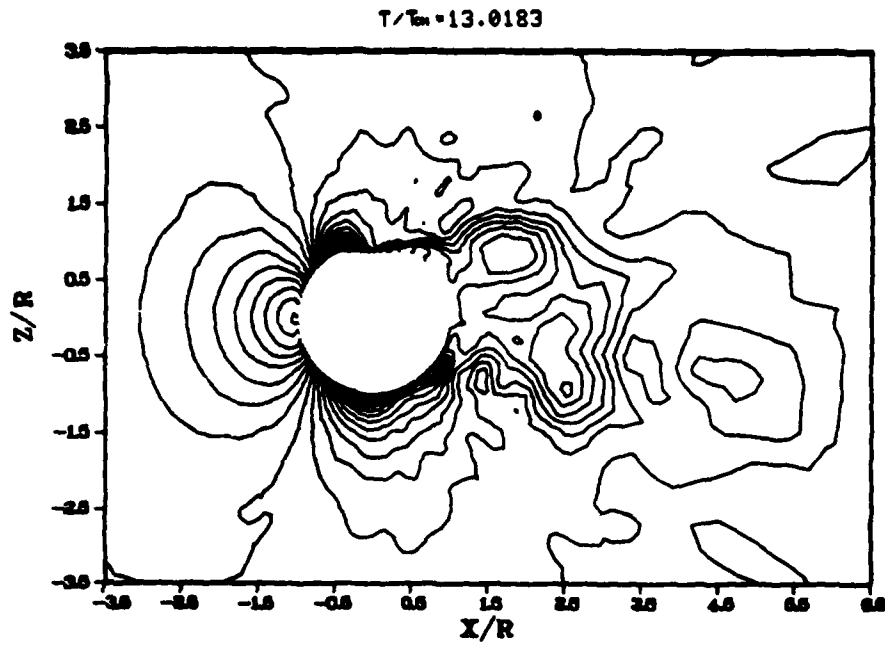


(a) $T/T_{CH} = 5.1488$

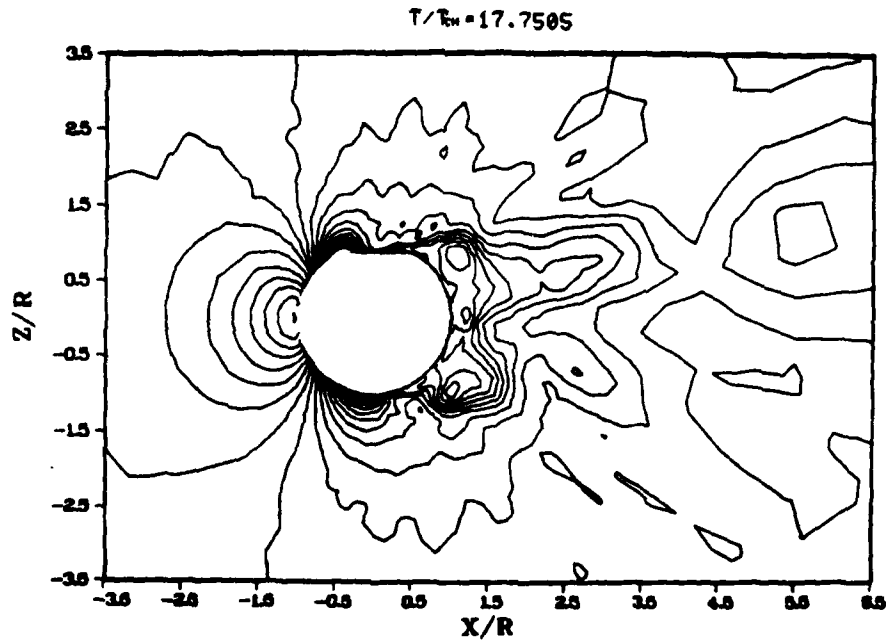


(b) $T/T_{CH} = 9.1799$

Figure 21. Density Contours Around the Turret Shoulder at Different Times.



(c) $T/T_{CH} = 13.0183$



(d) $T/T_{CH} = 17.7505$

Figure 21. (Concluded) Density Contours Around the Turret Shoulder at Different Times.

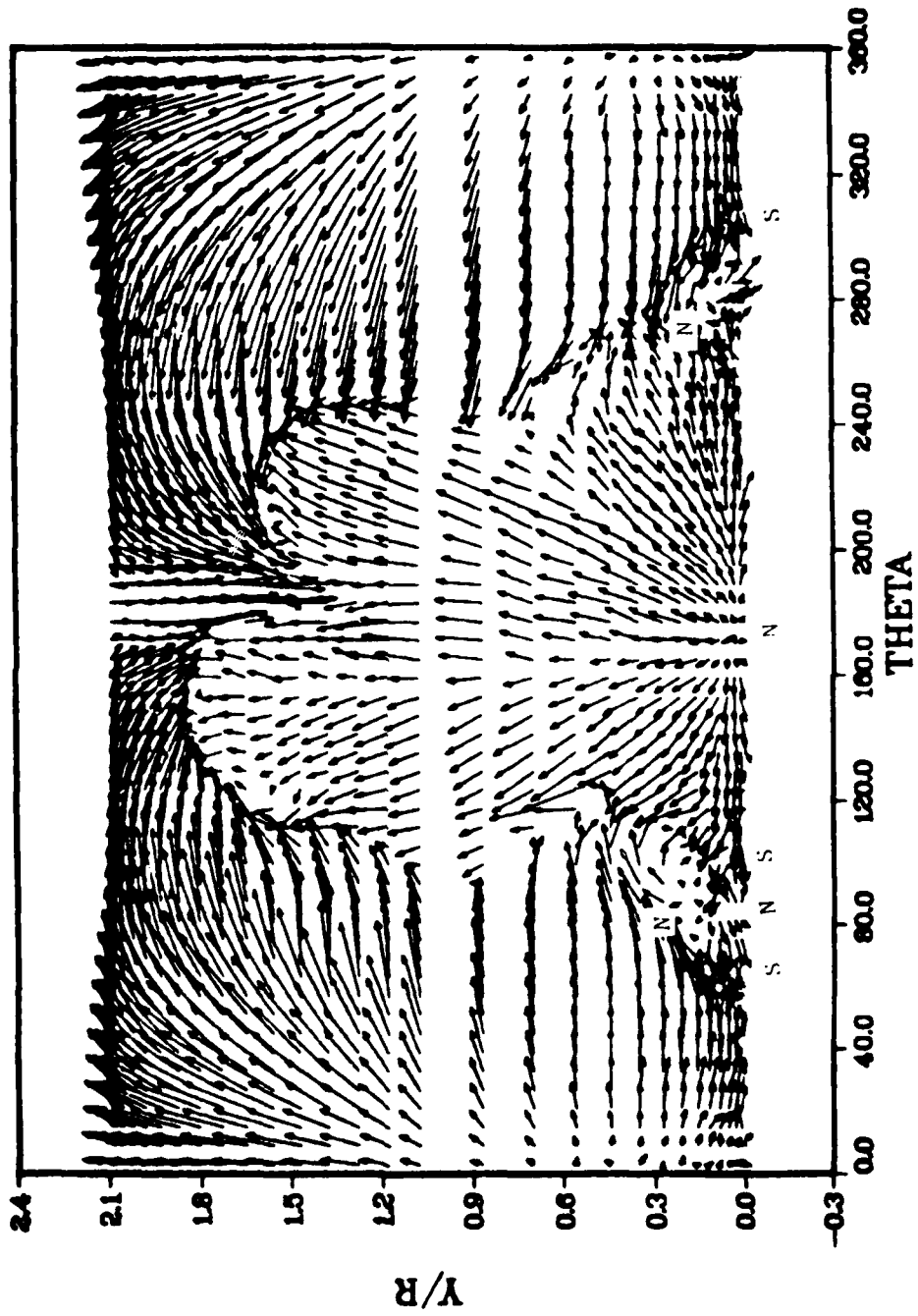


Figure 22. Instantaneous Limiting Streamline Pattern on the Turret Surface.

Finally, these limiting streamline patterns offer a precise description of the downstream flow. The situation is similar to flow past a hemisphere cylinder at 90° incidence. The separation line around the turret passes through the singular points, indicating a close-type of separation. This registers an inaccessibility of the outer flow to the near wake region^[19]. This interpretation follows logically from the steady state separated flow. However, the periodic mass exchange due to unsteady effects is evident

SECTION 5
CONCLUSIONS

An efficient numerical procedure is successfully accomplished for the three-dimensional separated flow around a turret. An adequate description of flow structure is obtained and an endorsement of a topological criteria is presented. For a free stream Mach number of 0.55 and a Reynolds number of 10.3×10^6 /meter, good comparison is established between our computed results and the experimental data for both the pressure distribution and levels of RMS density fluctuations.

REFERENCES

1. Sedney, R. and C. W. Kitchens, "The structure of three-dimensional separated flow in obstacle, boundary layer interaction," AGARD-CP-168, 1975.
2. Westkaemper, J. C., "Turbulent boundary layer separation ahead of a cylinder," AIAA Journal, Vol. 6, No. 7, July 1968, pp. 1352-1355.
3. Farivar, Dj., "Turbulent uniform flow around cylinder of finite length," AIAA Journal, Vol. 19, No. 3, March 1981, pp. 275-281.
4. Korkegi, R. H., "Survey of viscous interactions associated with high Mach number flight," AIAA Journal, Vol. 9, No. 5, May 1971, pp. 771-784.
5. Dolling, D. S. and S. M. Bogdonoff, "Scaling of interactions of cylinders with supersonic turbulent boundary layer," AIAA Journal, Vol. 19, No. 5, May 1981, pp. 655-657.
6. Peake, D. J. and M. Tobak, "Topology of two-dimensional and three-dimensional separated flows," AIAA Paper No. 79-1480, AIAA 12th Fluid and Plasma Dynamics Conference, Williamsburg, Virginia, 23-25 July 1979.
7. Hunt, J. C. R., C. J. Abell, and J. A. Peterka, "Kinematical studies of the flow around free or surface mounted obstacle; applying topology to flow visualization," J. Fluid Mechanics, Vol. 86, (1), 1978, pp. 179-200.
8. Wang, K. C., "Separation of three-dimensional flow," Report No. MML TR-76-55C, Martin-Marietta Laboratories, August 1976.
9. Maskell, E. C., "Flow separation in three-dimensions," RAE Aero report 2565, November 1955.
10. Shang, J. S., "Oscillatory compressible flow around a cylinder," AIAA Paper No. 82-0098, AIAA 20th Aerospace Sciences Meeting, 11-14 January 1982, Orlando, Florida.
11. DeJonckheere, R. K., J. J. Russell, and D. C. Chou, "High subsonic flow field measurements and turbulent flow analysis around a turret protuberance," AIAA Paper No. 82-0057, AIAA 20th Aerospace Sciences Meeting, 11-14 January 1982, Orlando, Florida.
12. Morrisett, E. L. and D. J. Bushnell, "Evidence of embedded vortices in a three-dimensional shear flow," AIAA Journal, Vol. 19, No. 3, March 1981, pp. 400-402.

REFERENCES (Concluded)

13. Baldwin, B. S. and H. Lomax, "Thin layer approximation and algebraic model for separated turbulent flows," AIAA Paper No. 78-257, AIAA 16th Aerospace Sciences Meeting, 16-18 January 1978, Huntsville, Alabama.
14. Shang, J. S., P. G. Bunning, W. L. Hankey, and M. C. Writh, "Performance of a vectorized three-dimensional Navier-Stokes code on a CRAY-1 computer," AIAA Journal, Vol. 18, No. 9, September 1980, pp. 1073-1979.
15. Shang, J. S., "Numerical simulation of wing-fuselage interference," AIAA Paper No. 81-0048, AIAA 19th Aerospace Sciences Meeting, 12-15 January 1981, St. Louis, Missouri.
16. MacCormack, R. W., "The effect of viscosity in hypervelocity impact cratering," AIAA Paper No. 69-354, 31 April - 2 May 1969, Cincinnati, Ohio.
17. Rose, W. C., "Measurement of aerodynamic parameters affecting optical performance," AFWL-TR-78-191, March 1979.
18. Rose, W. C., J. E. Craig, and K. R. Raman, "Nearfield aerodynamic and optical propagation characteristics of a large scale turret model," AFWL-TR-81-28, Air Force Weapons Laboratory, Air Force Systems Command, Kirtland AFB, New Mexico 87117.
19. Wang, K. C., private communication, 1982.

**DA
FILM**